ISSN: 2175 9146

JOURNAL OF AEROSPACE TECHNOLOGY AND MANAGEMENT

VOLUME NO. 16
ISSUE NO. 1
JANUARY - APRIL 2024

ENRICHED PUBLICATIONS PVT. LTD

**S-9, IInd FLOOR, MLU POCKET,
MANISH ABHINAV PLAZA-II, ABOVE FEDERAL BANK,
PLOT NO-5, SECTOR-5, DWARKA, NEW DELHI, INDIA-110075,
PHONE: - + (91)-(11)-47026006**

ISSN: 2175 9146

Journal of Aerospace Technology and Management

Aims and Scope

The Journal of Aerospace Technology and Management (JATM) is an open-access journal devoted to research and management on different aspects of aerospace technologies.

For all accepted manuscripts, the correspondence author will be asked to contribute with the Article Processing Charge, which will be applied to editorial services that support the publishing process, like editing, proofreading, indexing and dissemination.

The value is fixed per article, independent of its length and is R$ 800,00 (in Brazilian reais) or U$300,00 (in American dollars). In exceptional cases, the editorial board may waive a contribution upon reasonable request.

JATM accepts manuscripts already published in preprint, considered reliable by the editorial committee, and must be informed in the Open Science Compliance Form that must be submitted as a supplementary file to the Manuscript.

ISSN: 2175 9146

Journal of Aerospace Technology and Management

EDITORS IN CHIEF

ISSN: 2175 9146

Journal of Aerospace Technology and Management

(Volume No. 16, Issue No. 1, January - April 2024)

Contents

Formation of a Regionally Oriented Structure and Number of the Airline's Helicopter Fleet Based on Consumer Preferences of Customers

Yuriy Krivolutsky1,*

1. Moscow Aviation Institute – Management and marketing of high-tech industries – Moscow,

ABSTRACT

The aim of the work is to develop conceptual directions for the structure formation and the number of airline's fleet based on satisfying consumer preferences of enterprises-customers of helicopter operations. The helicopters currently in operation cannot fully satisfy the requirements of customers in terms of their flight technical and economic characteristics, which leads to a decrease in their use and it negatively affects the economy of the airline and corresponding economic region. There is a real need to update and expand the type and fleet of Russian-made helicopters, which will better meet the requirements of the helicopter operations market. To solve it, a helicopter manufacturing enterprise needs to carefully study the market requirements for existing and new types of helicopters, its volumes, formation trends, prices, operating costs, service systems, etc. The work presents a model that makes it possible to formulate for each airline the need for helicopters of various types and specializations for each year of the forecasting period has been developed, depending on the dynamics of changes in the level of socio-economic development of the region and the corresponding changes in the airline's flight operations, considering the effective demand. It also makes it possible to predict promising types and helicopter fleet.

Keywords: Airline; Aerial work; Helicopter fleet; Promising type; Market requirements.

INTRODUCTION

One of the main features of the Russian helicopter fleet is the regionality of its basing. Basically, up to 70% of the fleet is concentrated in industrially underdeveloped and climatically harsh regions. The main goal of the development of these regions is the creation and further development of the fuel and energy complex (FEC). These are the regions of the North, Siberia and the Far East. There are about two-thirds of the helicopter airlines there. Helicopters perform, at the request of customers, various types of work, the volume and nature of which vary depending on the region, its economic orientation and degree of economic development of the territory by one or another customer (Calado et al. 2019; Mustaev et al. 2021). Table 1 shows the distribution of flight hours on helicopters between the main customers of helicopter operations (Fomin 2019).

Table 1. Distribution of helicopter operations by main customers.

Customers	Share of flying hours in the total flying hours of the helicopter fleet, %
Vertically integrated oil companies, oilfield services and petrochemical companies	58
State and regional customers	14
Construction companies	11
Energy companies	9
Transport companies	6
Other	2

Source: Elaborated by the authors using data from Fomin (2019).

As we can see from the data in e Table 1, the main customers of helicopter services are enterprises of the fuel and energy complex. Among the main types of work, one can single out the transportation of goods, passengers, air patrolling and sanitary transportation.

Enterprises-customers of helicopter operations indicate that for a wider use of helicopters it is necessary that their type is more consistent with the nature of the work performed and the cost of their operation should be reduced. Analysis of the structure of the Russian helicopter fleet in these regions shows that the bulk of aviation work is carried out by medium-class helicopters of Mi-8 / Mi-17 type. For the light helicopters of Mi-2 type and heavy helicopters Mi-26, there is a smaller amount of work (Butov 2018). The state of the existing fleet of Russian helicopters, namely, its aging and decommissioning, with a significant share of new foreign light helicopters, indicates that there is a real need to update and expand the type and fleet of Russian-made helicopters in airlines, which will be more consistent with the requirements of the market for helicopter operations (Butov 2018; Kuprikov et al. 2019). The problem of forming a promising type and fleet of helicopters in airlines poses a task for a helicopter manufacturer to independently thoroughly study the market requirements for new helicopters, its volumes, formation trends, prices, operating costs, service systems, etc. (Kochergina 2017). Conducting marketing research and, on their basis, formation of a regionally oriented competitive strategy for the development of new helicopters will reduce the risk of creating an unacceptable helicopter for the market, more efficiently use its own resources, determine optimal volumes and terms of production and, ultimately, outstrip foreign competitors (Keivanpour and Ait Kadi 2017; Tikhonov 2020). On the basis of these studies, it is realistic to create a model for the formation of the structure and number of the airline's helicopter fleet, using it becomes possible to determine the need for helicopters of various takeoff weights and specializations for each year of the forecasting period, taking into account forecast models of the socio-economic development of the region and the dynamics of changes in the volume of flight work on each regional airline. A number of scientific works of the following authors are devoted to the development of the helicopter fleet and the helicopter services market: RUCON AFK (2022), Baklanov (2007), Demin (2014), Kravchenko (2013), Maslov and Krivolutsky (2009), Lesnichiy (2009), Litvinov (2003), Pripadchev and Sultanov (2009), Smirnova and Erdnieva (2020) and Sobolev (2018). The high

relevance of such scientific research is explained by the insufficient scientific elaboration of this problem area.

METHODOLOGY

Intensive progressive development of a helicopter company can be ensured only through the accumulation of scientific knowledge obtained in the process of creating new helicopters, realizing which, in Russian and foreign markets, receives new incentives for its development (Droff and Bellais 2016; Kotler and Armstrong 2017). Extensive development, as a rule, is inherent in the processes of creating various modifications. For example, Mi-8 helicopter has at least about 10 different modifications.Currently, the problems of selling new helicopters and updating the helicopter fleet have become more acute. Under these conditions, it is not realistic to maintain the previously won market shares and ensure a high level of competitiveness of helicopters based on the assumed homogeneity of demand. A strategic decision could be the maximum possible adaptation of existing and new development helicopters to the requirements of various market segments and the manufacturing of products of diverse characteristics and, thus, stimulating demand. To solve this problem, it is advisable to carefully analyze the market for helicopter operations and their customers in order to identify target segments and then study the segments themselves according to various characteristics (Shatova 2017). Under the segmentation of the helicopter operations market, we will understand the task of dividing a set of helicopter operations, as a certain set, into segments that have common main characteristic features at different levels according to the depth of segmentation.

This will make it possible to establish the territorial-geographical and regional distribution of helicopters, the main customers of helicopter operations, the types of work, etc. Helicopter segmentation levels can be arranged in the sequence shown in Table 2.

Table 2. Helicopter segmentation levels.

Levels	Segmentation levels
1	Territorial-geographical
2	Regional
3	Intra-regional economic zones
4	Main service industries
5	Main types of work
6	Scope of work and its stability
7	Dominant loading parameters by type of work
8	Natural and climatic conditions for the performance of work

Source: Elaborated by the authors.

An example of a structural grouping of the helicopter operations market is shown in Table 3.

Table 3. Structural grouping of the helicopter operations market

Tier Segmentation Options	Helicopter market segments		
Territorial-geographical	North	Siberia	Far East
Regional	Northwest	West Siberian, East Siberian	East
Intraregional business zones	Arkhangelsk, Murmansk, Syktyvkar, Ukhta	Tyumen, Surgut, Khanty-Mansiysk, Nefteyugansk, Krasnoyarsk	Yu zhno-Sakhalinsk, Okha, Khabarovsk, Vladivostok
Main service industries	FEC, Geology, Medicine	FEC, Medicine	Geology, Fisheries and Forestry, Medicine
Main types of work	Transportation of goods, passengers, patrolling, sanitary transportation	Transportation of goods, passengers, patrolling, sanitary transportation	Transportation of passengers, patrolling, forest protection, sanitary transportation
Possible scope of work and their stability	In accordance with the development of the region's economy. Permanent and periodic	In accordance with the development of the region's economy. Permanent and periodic	In accordance with the development of the region's economy. Permanent and periodic
Prevailing helicopter loading parameters by type of work	Distribution of cargo transportation (passengers) and the number of patients by range zones, patrolling time	Distribution of cargo transportation (passengers) and the number of patients by range zones, patrolling time	Distribution of cargo transportation (passengers) and the number of patients by range zones, patrolling time
Natural and climatic conditions of work performance	Unprepared sites, low temperatures in winter, high in summer, polar night, flights over the sea	Unprepared sites, low temperatures in winter, high temperatures in summer, flights over the tundra and taiga	Unprepared sites, low temperatures in winter, high in summer, flights over the sea, hills, tundra

Source: Elaborated by the authors.

A helicopter company can act in several market segments, developing a separate offer for each of them in the form of a new type of helicopter (Crivelli and Rubini 2020; Xinyu Zhang and Xinai Zhang 2020). This refers to the lowest level of segmentation: types of work and their characteristics. The task is that according to the results of the study, the developer must choose: which market segments are most attractive to him in terms of potentially high demand, and how many of them are proposed to borrow from the point of view of the company's capabilities (Kotler and Armstrong 2017). The most profitable segment should be distinguished by a potentially high level of sales of helicopters and their annual load in airlines, a low level of competition from other market participants and be quite attractive from an economic point of view for helicopter operators and helicopter customers.Enterprises - customers of helicopter work differ in the types and volumes of ordered work, the dimensions of the goods transported, the number of passengers, the method of

performing work (for example, gravimetric survey by geologists), the necessary suitability of the helicopter to perform a particular work (for example, sanitary transportation), the frequency of work, the solvency, etc. The nature of these works varies depending on the region, within the regional economic zones and the degree of economic development of the territory by one or another customer. This determines the main requirements on the part of

customers for the main technical and economic indicators of helicopters, such as payload, speed and flight range. The marketing theory assumes that in terms of their level these indicators should correspond to the modern market evolution of Russian air transport market, which implies continuous modernization and renewal of the helicopter fleet.In the case when FEC enterprises, as well as enterprises associated with the exploration and production of minerals (geology), prevail among the main customers, it is interesting what type of helicopters they require at different stages of the technological processes of territory development inherent in these industries (Table 4).

Table 4. Types of helicopters used by stages of the technological process of territory development at FEC and geology enterprises.

Stage of technological process of territory development	Predominant type of work		Types of helicopters used	
	FEC	Geology	FEC	Geology
Mineral exploration	Freightage	Gravimetric survey	Heavy	Heavy, light and medium
Industrial development of deposits	Transportation of people and goods at the same time	Transportation of people and goods at the same time	Heavy and medium	Light and medium
Field operation	Air patrols	Transportation of people, transportation of people and goods at the same time	Light and medium	Light and medium

Source: Elaborated by the authors.

The data given in the Table 4 show that in the initial stages of economic development of the territory for the exploration and production of energy resources, the use of heavy transport helicopters (transportation of equipment, drilling rigs) prevails, in the future, the joint transportation of people and cargo begins to prevail and medium and light helicopters are used. In the field operation mode, the main type of helicopter work is air patrolling of pipelines.

Since we have already determined that potential customers of helicopter services will be enterprises of FEC, we will study market segments primarily from the point of view of meeting the needs of these enterprises.

We define a set of possible helicopter models using the defining property P(X), common to all elements of the set, and denote (Eq. 1):

$$X=\{x \mid P(x)\} \quad (1)$$

As a defining property for helicopters performing various types of work, we take the mass of the payload *Glp* , transported over a certain distance. Then Eq. 1 can be written as follows (Eq. 2):

$$X=\{G_p^l \mid P(G_p^l)\} \quad (2)$$

To visualize the relation between subsets A, B, C, D (types of work) of any universe U (set of admissible objects) we use Euler circles. Crossing A ∩ B ∩ C ∩ D is a set of elements belonging to A, B, C, D simultaneously by the defining property: Glp (in Fig. 1, there is the shaded area) (Droff 2017; Vascik et al. 2018).

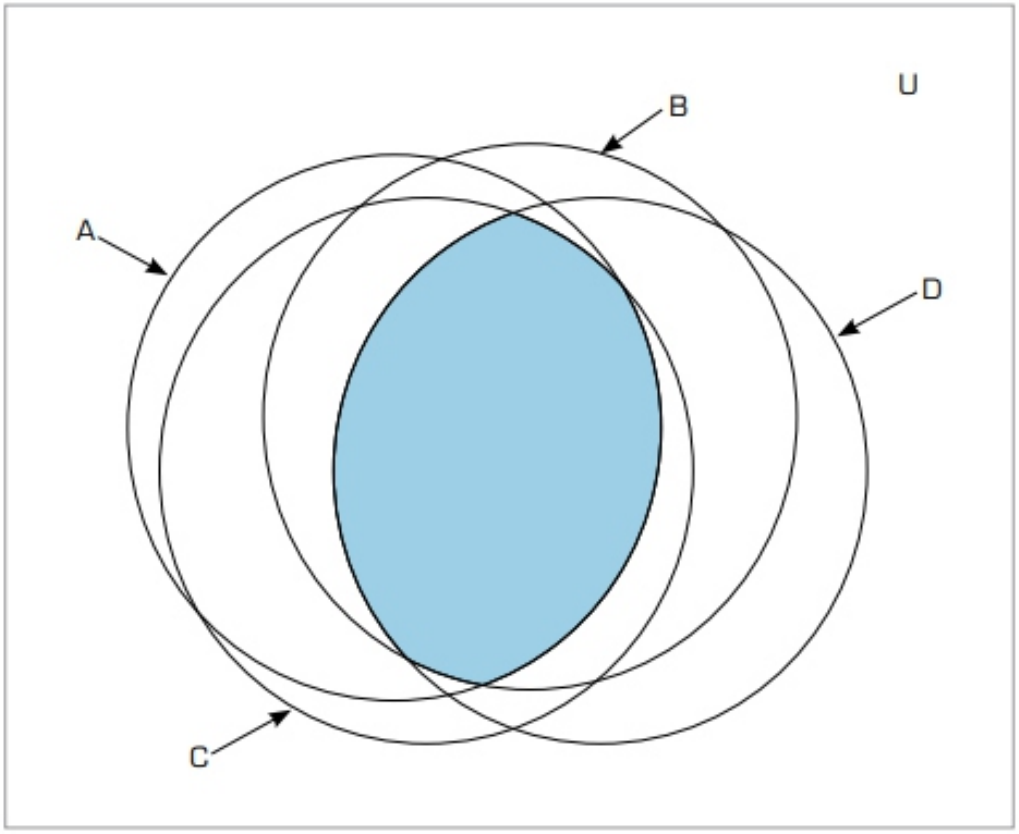

Source: Elaborated by the authors.

Figure 1. Image of the relation between individual types of work on the defining property To identify the defining property P(Glp) helicopters, it is necessary to consider the value of this characteristic for the works most inherent in the enterprises-customers of FEC.

RESULTS

Analysis of the segment structure of the helicopter market by characteristic quantitative features

When studying the segmental structure of the market for air transport operations performed with the help of helicopters, quantitatively homogeneous aggregates can be distinguished using a small number

of features. These include the mass of cargo transported and the number of passengers by range zones, the characteristics of loading and the range of helicopter flights during air patrols and sanitary transportation. These data are presented in Table 5.

Analyzing the data on the transportation of goods with their distribution by mass, it can be noted that 82% of goods have up to 2000 kg, and in 68-83% of cases they move at a distance of up to 400 km.The mentioned data about passenger traffic indicates that a significant share (up to 35%) is the transportation of small groups of passengers (up to 7 people), and a significant share (59%) are the groups of 8-17 people. For the transportation of this category of passengers, customers are encouraged to use Mi-8 helicopter, although in this case it would be more economical to offer them a helicopter of an "intermediate" class, ideal for this category. Such a helicopter could be used for flights of even small groups of passengers (5-7 people) at a distance of over 400 km.

Table 5. Types of helicopter operations and their characteristics for fuel and energy enterprises in the West Siberian region of the Russian Federation

Types of works	Cargo weight, kg	Flight range up to 400 km, %	N° passengers, people	N° patients + service staff, people
Carriage of goods	Up to 500 (30%)	75		
	501-1000 (17%)	68		
	1001-1500 (19%)	82		
	1501-2000 (16%)	83		
Transportation of people		68	1-4 (18%)	
		80	5-7 (17 %)	
		88	8-17 (59%)	
Aerial patrol	Up to 100	80-100	1-2	
Sanitary transportation	40-150 (equipment)	70-90		3-4 sedentary patients, 1-3 bed-patients + 1-2 medical staff (70%)
				2-6 sedentary patients, 2-4 bed-patients + 4-6 medical staff (30%)

Source: Elaborated by the authors.

For ambulance flights, helicopters of light and medium classes are mainly used. For light helicopters, the typical load is three sedentary patients and one bed-patient. They are accompanied by one or two doctors. Middle-class Mi-8 helicopters, as a rule, carry 3-4 sedentary patients and 3 bed-patients. At the same time, there is a medical team on board, sometimes up to 6 people. From an economic point of view, this is ineffective, but there is no smaller helicopter designed for such a payload. Mi-8 helicopter is most often used for long-range flights, even with a small number of patients. Almost 90% of sanitary flights are carried out in the range of distances up to 400 km. Knowledge of these values makes it possible to

optimize the size and payload within the 1500-2000 kg range of a special ambulance helicopter, which will allow the use of helicopters at lower costs and provide the population with more medical care.

Helicopters are used for almost all types of patrolling: patrolling forests in order to detect fires without rescuers and patrolling forests with a group of rescuers-firefighters for emergency extinguishing of detected fires, forest inspections for pathology (detection of contaminated areas), patrolling river and sea areas (fish breeding), reconnaissance of schools of fish in the ocean, ice reconnaissance and compilation of ice maps, pilotage of ships in ice, patrolling of oil and gas pipelines and roads, patrol, search and rescue operations. Helicopters of light and medium classes are used to carry out patrol work. The average patrol time for

light helicopters is 2.5 hours on average, while for Mi-8 helicopters it is about 4.5 hours. Mi-8 helicopters have a significant share of patrol flights due to the possibility of providing a longer duration and range of patrols through the use of additional tanks. It is economically ineffective, but customers have not got another choice. The only way the customers can compensate for the high costs of using Mi-8 helicopters during patrol flights is the execution of parallel tasks for the delivery of passengers and cargo to points lying along the patrol route or not far from them.

The results of the analysis indicate that the considered segments of the work performed by helicopters have much in common. It has a flight range of up to 400 km, the mass of the transported cargo is in the range of 1.5-2 tons and there are 8-17 passengers. The helicopters currently in operation cannot fully satisfy the requirements of customers in terms of their flight technical and economic characteristics.Conceptual directions for updating the helicopter transport complex

We single out two conceptual directions of the helicopter fleet renewal strategy: adaptation of the existing helicopter fleet to market requirements and development of a new type of helicopters.

Adaptation

Customer orientation is a kind of “customer fit”, i.e. this is a search in its activities for the direction where the company can prove itself in the best way compared to competitors. Many companies, especially those operating in the industrial equipment market, carefully divide their clients into multiple segments due to its limitations, thereby achieving the ability to deliver products and services tailored to the place. For example, Boeing company considers each of its customers a separate segment of the market. Such an account of the requirements of each specific consumer of new technology turns out to be very effective. Since all the considered segments cannot fully satisfy these indicators, it is proposed to adopt a multi-purpose helicopter as a compromise solution, which, in its basic basis, will be specialized in performing a certain type of work and, at the same time, will be able to perform other types of work quite efficiently. Modifications of Mi-8 helicopters in transport, passenger and ambulance versions can serve as an example. In modern conditions, in order to retain market share and stimulate

sales, a more accurate determination of the desires of consumers in various market segments is required. If the basic model is available, it is possible to create modifications of a deeper level, which differ not only their purpose, but also have additional features (options) that allow modifying the equipment and choosing the option that is most suitable for the purposes of the operator. These can be various equipment configurations, engine types, flight performance, maintenance options, repairs, etc., which are most suitable for performing the types of work prevailing in this particular segment, in this airline, and to a greater extent satisfying customers. The scheme of such basic unification is shown in Fig. 2.

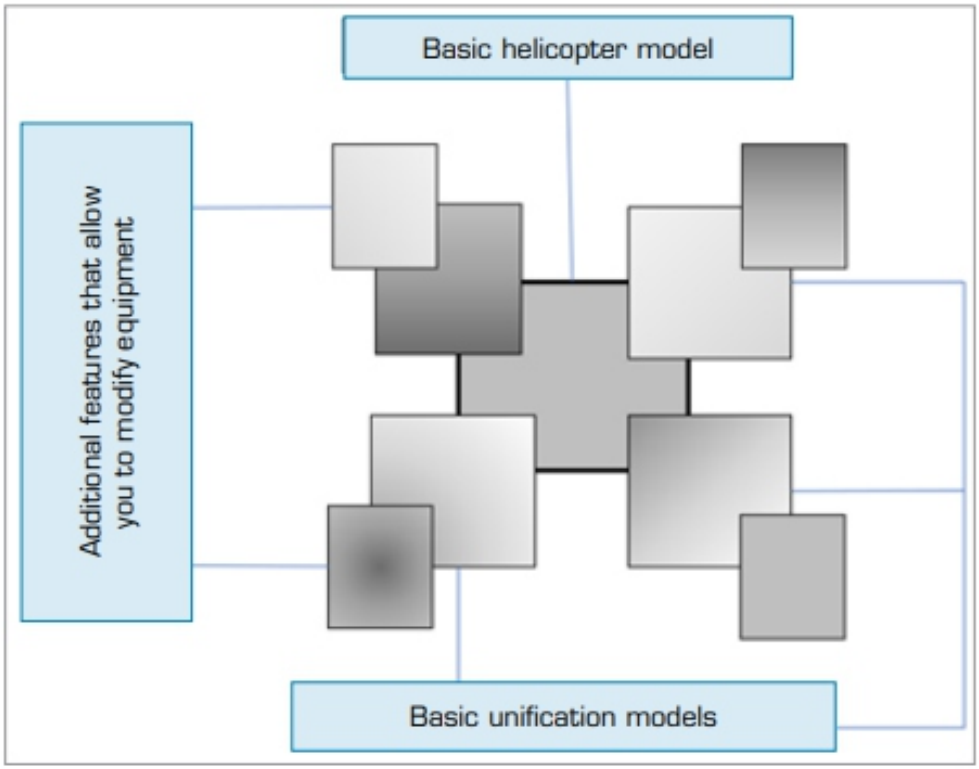

Source: Elaborated by the authors.

Figure 2. Scheme of combining the characteristics of helicopters based on the development of the basic version and additional features that allow the modification of equipment.

For an airline, as a buyer of helicopters, with limited financial resources, one of the economic conditions for the implementation of such a strategy is the fulfillment of the following ratio (Eq. 3):

$$\sum_{i=1}^{n} \quad (P_{bas} + \Delta P_i) \times N_i \leq P_{univ} \times N_{univ} \qquad (3)$$

where:

Puniv is the price of a helicopter, universal in its configuration, “for all occasions”, for all segments, rub.; Pbas is the base price of a helicopter in a standard configuration, excluding additional “fitting” of a helicopter to the requirements of a certain segment, rub.; ΔPi is the surcharge to the base price of a helicopter for “fitting” a helicopter to the requirements of consumers of a certain i-th segment, rub.;

Nuniv is the volume of purchases of helicopters, universal in their configuration, excluding market segmentation,pcs.; Ni is the volume of purchases of helicopters, completed taking into account the requirements of consumers of each i-th segment, pcs.; n is the number of market segments considered.

As an example, we can cite the fact that at one time, during the first three years of serial production of Boeing-707 aircraft, Boeing company delivered seven modifications to the market, differing from each other in wingspan, fuselage length or engine types. Thus, the installation of the Rolls-Royce engine instead of American-made engines contributed to the promotion of the

Boeing-707 aircraft to the British market. When creating the Airbus, European firms proposed three variants of this aircraft, each of which was optimized for a certain range and a certain passenger flow, which met the requirements of various customer groups.

It should be noted that it takes less time to create modifications than to develop a new aircraft.Development of a new type of helicopterWhen choosing the parameters of a new helicopter as a multi-purpose system, it is necessary to use its efficiency indicator as the main criterion. Two approaches are possible here. Firstly, the efficiency of a multi-purpose system can be estimated as the sum of the efficiencies of performing single tasks (the rule of integral evaluation), and secondly, it can be estimated as the limiting efficiency of performing single tasks (the rule of guaranteed evaluation).We consider a model for the formation of the structure and number of helicopter fleets in an airline, taking into account the consumer preferences and forecasts of socio-economic development of the regions, determining the volume of flight work of the regional airline. In the proposed economic-mathematical model as a criterion for the optimality of the structure of the helicopter fleet, we take the maximum return on invested capital for the forecasting period (efficiency) (Eq. 4):

$$Eff = \frac{P}{E} \rightarrow max \qquad (4)$$

where:

P is the profit from the operation of various types of helicopters for various types of work; E is the amount of expenses for the purchase, operation and repair of various types of helicopters in the airline.In turn, P and E are defined as follows (Eqs. 5 and 6):

$$P=\sum_{t=t_0}^{T} \sum_{n=1}^{m} \sum_{i=1}^{S} Q_{gener}(t)*\gamma_i * \eta_i * P_i \frac{1}{(1+\alpha)^{T-t_0}} \qquad (5)$$

where:

Qgener(t) is the annual volume of all types of airline work in flight hours in year t; γi is the share of the i-th work in the total volume of work of the airline; ηi is the specific weight of the i-th work attributable to the n-th type of helicopter; Pi is the profit received by the airline from performing the i-th job of n-th type

of helicopter; m is the number of types of helicopters available in the airline; S is the number of types of work performed.

$$E = \sum_{t=t_0}^{T} \sum_{n=1}^{m} \{C\ [\Phi_P\ (m,t)] + O[\ \Phi_P\ (m,t)] + R[\Phi_P\ (m,t)]\} \frac{N_n\ (t)}{(1+\alpha)^{T-t_0}} \quad (6)$$

where:

C is the capital expenses for the purchase of helicopters; O is the helicopter operating costs; R is the helicopter repair costs; Φp(m,t) is the array of parameters that determine the amount of costs (prices of helicopters, their equipment, operating features, etc.); α is the standard for bringing different costs; t0, T is the first and the last years of the forecast period, respectively; Nn(t) is the number of n-type helicopters used to perform a certain amount of work in year t.The system of restrictions is the following (Eq. 7 and 8):

$$\sum_{n=1}^{m} \quad \sum_{i=1}^{S} \quad N_p\ (t)\ \tau_i\ (t) \geq Q_{gener}(t) \quad (7)$$

$$\sum_{n=1}^{m} \sum_{i=1}^{c} C\ [\Phi_p\ (m,t)]\ N_n\ (t) \leq \bar{C}\ (t) \quad (8)$$

In Eq. 7 and 8, we use the following notation:τi(t) are the flying hours of n-type helicopter in year t at the i-th job; C (t) is the amount of capital investments allocated by the airline for the purchase of helicopters in year t.According to Eq. 7, in each year of the prospective period, the helicopter fleet must perform the amount of work Qgener(t), determined by exploratory or normative forecasting methods taking into account the indicators of socio-economic development of the region.Equation 8 stipulates that the volume of capital investments for the purchase of helicopters should not exceed the value C (t) allocated for this in the year t.

As a result of using this model, it becomes possible to determine the need for helicopters of various takeoff weights and specializations for each year of the forecasting period, taking into account the dynamics of changes in the volume of flight operations of each airline.

It should be noted that the demand for various types of helicopters and their number obtained from this model is not the actual demand for helicopters, but the effective demand, which follows from the system of restrictions.The scope and content of airline operations in different regions and the composition of the main customers for helicopter operations may differ due to the fact that the regions have, as a rule, different sectoral structure, different rates and trends of their economic development (Regions of Russia; Socio-economic indicators 2023; Federal State Statistics Service 2015). Therefore, the efficiency of updating the type and fleet of helicopters in a regional airline and bringing them in line with market requirements may vary. On the basis of data on the socio-economic development of the regions, models for calculating the volume of airline flight operations in the region can be built. An example of building such a model is shown in Fig. 3.

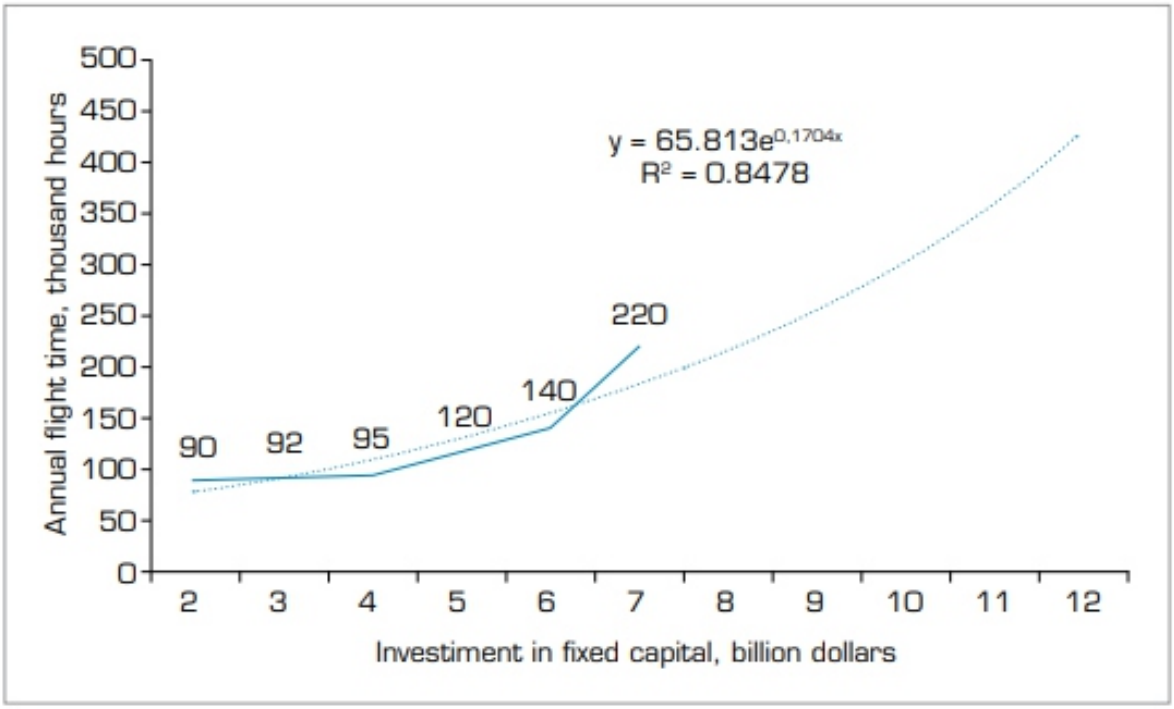

Source: Elaborated by the authors.

Figure 3. An example of determining predictive estimates of the total flying hours of an airline's helicopter fleet depending on investments in fixed assets in the region.For a developing helicopter company, such a parametric analysis for most Russian airlines will make it possible to more objectively judge the structure and size of the required type and fleet of helicopters, its expansion, saturation due to the creation of new models or modifications of existing helicopters and, accordingly, possible costs of development and serial production.

DISCUSSION

To ensure the successful operation of airlines in the near future, it will be necessary to update the type and fleet of helicopters and, on this basis, expand their use among existing and potential customers of helicopter operations. Due to the fact that 87% of Russian helicopter fleet is over 25 years old, the issue of replacing the most common Mi-8T(P) helicopter with its new modifications Mi-8AMT / MTV-1 and limiting the service life of Russian helicopters to 25 years is being intensively discussed. It is assumed that such a replacement will make it possible to load the production capacities of serial enterprises and ensure their technical re-equipment. As counterarguments, they cite the high flight safety characteristics of Mi-8T helicopters, financial difficulties with the acquisition of new helicopters and increase in the cost of their flying hour, which is unacceptable for airlines. Statistical data on the flight safety of Mi-8T (P) and Mi-8 MTV (AMT) helicopters indicate that the accident rate of the "old" Mi-8T helicopter (0.52*10-5) is significantly lower (2.4 times) than the more modern Mi-8MTV-1(AMT) (1.26*10-5).

The comparative values of the "risk of mortal injury" criterion for these helicopters are 0.17*10-5 and 0.93*10-5, respectively, i.e. according to this criterion, Mi-8T helicopter is 5.5 times safer than Mi-8MTV (AMT) helicopter. If we consider the economic aspects of the use of helicopters, it can be noted that the price of the new Mi-8 MTV (AMT) helicopter is about 10 times higher than that of Mi-8 T (P) helicopter and amounts to 550 million rubles, and the cost of a flight hour 1.7 times higher (Khudolenko 2014). With a lack of funds from helicopter operators due to low profitability of their business, high prices for new Russian helicopters and a limited range of helicopters produced today, airlines in their current state are not able to upgrade their fleet of helicopters.

From the point of view of expanding the areas of use of helicopters and effective loading of the helicopter fleet, it is necessary, on the basis of marketing research, to determine the consumer preferences of customers of helicopter services, a promising line of a model range of helicopters and their number for each type.

When analyzing the segment structure of the helicopter operations market, one can clearly see the desire of customers in most cases to use helicopters lighter than Mi-8 or the so-called "intermediate" class with a payload from 1.5 to 2 tons and a maximum take-off weight in the range of 4.5-5.5 tons (Fig. 4). They are much cheaper than Mi-8MTV helicopters and, at the same time, have high functionality. An example of foreign helicopters of this class is Bell-212, Bell-214, AW-139, S-76 helicopters (Eshel 2013; Kolesnikova and Kovalchuk 2021). Unfortunately, customers most often have to use Mi-8 medium-class helicopter for almost all cargo in the range over 500 kg, which significantly increases the cost of transportation.

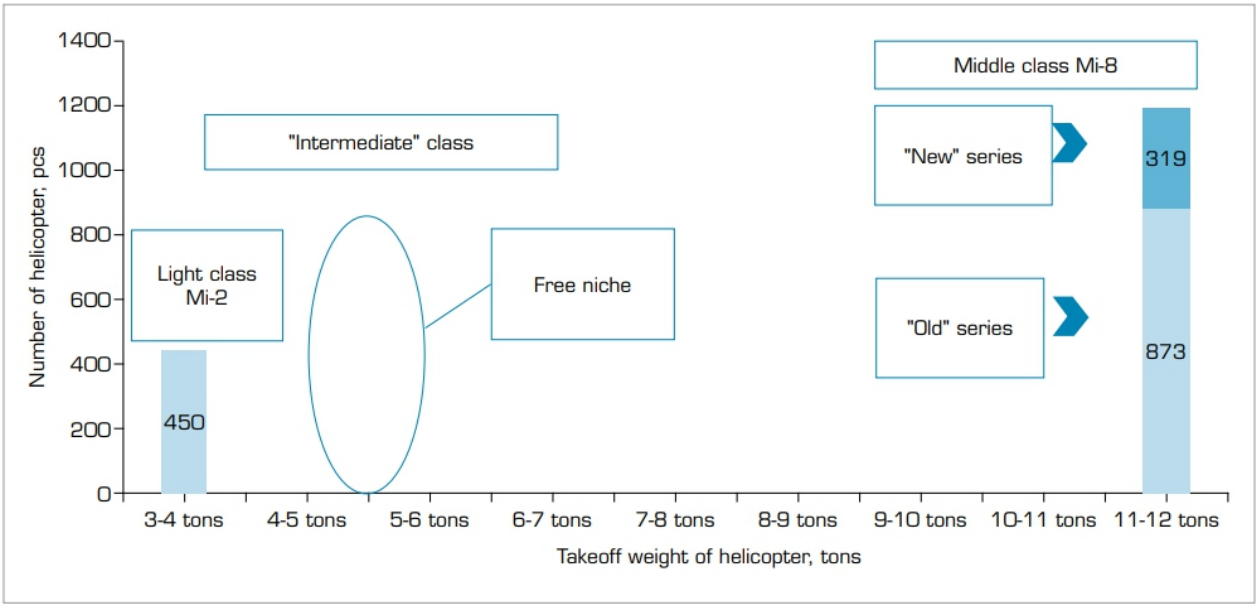

Source: Elaborated by the authors.

Figure 4. Distribution of the Russian fleet of the most common helicopters by take-off weight.

Taking into account the results of the analysis of trends and forecasts of the development of the national economy of Russia and the state of the helicopter fleet, it will make it possible to develop a realistic scenario for the formation of the structure and number of the renewed fleet of Russian helicopters and to optimize the presence of foreign manufacturers in it.

CONCLUSIONS

A meaningful formulation of the management task of a thorough study of the market requirements for new helicopters, from the point of view of meeting the needs of customer enterprises, has been formed. Marketing research of the characteristics of the work performed by customers will reduce the risk of creating a new type of helicopter that is unacceptable for the market, more efficiently use its own resources, determine the optimal production volumes and, ultimately, get ahead of foreign competitors.In accordance with the theory of sets, the mass of the payload Glp, transported over a certain distance, is taken as a defining property for helicopters performing various types of work. To identify the defining property P(Glp) of helicopters, we considered value of this characteristic for works that are most inherent in the enterprises-customers of FEC in the West Siberian region of Russia and in related industries that make up the elements of the infrastructure of the economic region: air patrolling and sanitary transportation.

The analysis showed that the considered characteristics of the work performed by various types of helicopters have much in common. Firstly, it has a flight range up to 400 km, the weight of the transported cargo is in the range of 1.5-2.0 tons and 8-17 passengers. The helicopters currently in operation cannot fully satisfy the requirements of customers in terms of their flight technical and economic characteristics.

In the near future, for existing helicopters, it is realistic to create modifications of a deeper level, differing in equipment configuration, engine type, flight performance, etc., which are most adapted to perform the types of work prevailing in a given airline and more fully satisfy customers.The most promising helicopter, capable to a greater extent of meeting customer requests for most types of work and, at the same time, being profitable for operators could be a helicopter of an “intermediate” class with a takeoff weight of 4.5-5.5 tons, highly competitive, promising sales and a real opportunity to renew the existing fleet of helicopters by partially replacing Mi-8 helicopters with a 25-year and more service life.

The model presented makes it possible to determine for each airline the need for helicopters of various types and specializations for each year of the forecasting period depending on the parameters of the socio-economic development of the regions and, accordingly, depending on the dynamics of changes in the airline’s flight operations, taking into account effective demand and, on this basis, to predict the number of a promising type and fleet of helicopters.

Increasing the availability and quality of air transport services for consumers can be achieved by developing and optimizing the fleet of modern aircraft, bringing the structure of the supply of air

transportation and aviation work to the structure of demand for them and reducing the cost of transportation.

CONFLICT OF INTEREST

The author declares no conflict of interest.

DATA AVAILABILITY STATEMENT

All data sets were generated or analyzed in the current study

FUNDING

Not applicable.

ACKNOWLEDGEMENTS

Not applicable.

REFERENCES

1. [RUCON AFK] (2022) [Civil helicopter market analysis by the results of the 1st half of 2022: Global civil and commercial helicopter market] [Internet]. In Russian. [accessed 2023 June 26]. https://afk.rukon.ru/analitika/post-1573/

2. Baklanov AG (2007) Market and marketing of aerospace products in conditions of instability. Moscow: Book House University.

3. Butov AM (2018) The market for civil aircraft products. Moscow: National Research University Higher School of Economics. Development center.

4. Calado EA, Leite M, Silva A (2019) Integrating life cycle assessment (LCA) and life cycle costing (LCC) in the early phases of aircraft structural design: an elevator case study. Int J Life Cycle Assess. 24(12):2091-2110. https://doi.org/10.1007/s11367-019-01632-8

5. Crivelli P, Rubini L (2020) 'Flying High in a Plane' Appellate Body Report, European Communities and Certain Member States–Measures Affecting Trade in Large Civil Aircraft. World Trade Rev 19(2):316-340. https://doi.org/10.1017/S1474745620000063

6. Demin SS (2014) [Helicopter building in Russia: trends of innovative modernization]. [Hum, Soc-Econ and Soc Sci] 12(3):49-53. In Russian. [accessed 2023 June 26]. https://cyberleninka.ru/article/n/vertoletostroenie-v-rossii-tendentsiiinnovatsionnoy-modernizatsii

7. Droff J (2017) The European military helicopter industry: Trends and perspectives. Econ Peace Secur J 12(1):20-27. https://doi.org/10.15355/epsj.12.1.20

8. Droff J, Bellais R (2016) Fleet management in European integration: the case of military helicopter

support. Def Sec Anal 32(1):19-35. https://doi.org/10.1080/14751798.2015.1130315

9. Eshel T (2013) Elbit Systems to address Indian helicopter market. Vayu Aerospace and Defence Review 2:74. [accessed 2023 June 26]. https://search.proquest.com/openview/089453dfbf9968ad089712f54fe6b7e4/1?pq-origsite=gscholar&cbl=2028820

10. Federal State Statistics Service (2015) [Socio-economic situation of the constituent entities of the Russian Federation]. In Russian. [accessed 2023 June 26]. http://www.gks.ru/free_doc/new_site/region_stat/sep_region.html.

11. Fomin SV (2019) [On the state of the Russian aircraft market and measures of state support for the renewal of the helicopter fleet of Russian airlines]. [XII Helicopter Forum "Company-operator activities as a mirror of the helicopter industry"]. In Russian. [accessed 2023 June 26]. https://helicopter.su/wp-content/uploads/2019/11/o-sostoyanii-rossijskogo-rynka-vt.pdf

12. Keivanpour S, Ait Kadi D (2017) Modelling end of life phase of the complex products: the case of end of life aircraft. Int J of Prod Res 55(12):3577-3595. https://doi.org/10.1080/00207543.2017.1308577

13. Khudolenko OV (2014) [Ways to improve the efficiency of operation of the fleet of domestic helicopters]. Aviation Explorer [Internet]. In Russian. [accessed 2023 June 26]. https://www.aex.ru/docs/9/2014/12/26/2171/print/

14. Kochergina AB (2017) Strategic marketing planning based on segment sustainability. Ec Syst 10(4):65-67.

15. Kolesnikova A, Kovalchuk J (2021) Modernization or New Engineering: Models of Leadership in the Global Civil Aviation Market. In: Stepnov I, editor. Technology and Business Strategy. Cham: Palgrave Macmillan. https://doi.org/10.1007/978-3-030-63974-7_6

16. Kotler PT, Armstrong G (2017) Principles of Marketing, Global Edition. Harlow: Pearson.

17. Kravchenko AV (2013) [Some issues of aircraft fleet optimization methodology]. Resh Read 1(17):364-365. In Russian Kuprikov MY, Rabinskiy LN, Kuprikov NM (2019) Business objective for the life cycle of aircraft. INCAS Bull 11(Spe):153-162. https://doi.org/10.13111/2066-8201.2019.11.S.15

18. Lesnichiy IV (2009) [Organizational and economic justification for the development of the helicopter services market]. (doctoral dissertation). Moscow: State Institute of Management. In Russian.

19. Litvinov NN (2003) [Technology for substantiating the strategy for re-equipping an aviation company with aircraft (on the example of local airlines and the conditions of the Tyumen region)] (doctoral dissertation). Moscow: Moscow Aviation Institute. In Russian.

20. Maslov AD, Krivolutsky YV (2009) [The method of forming the structure and number of the helicopter fleet based on predictive models for the development of the region]. [Bull Moscow Av Inst] 16(6):4-4. In Russian.

21. Pripadchev AD, Sultanov NZ (2009) [Optimization of the aircraft fleet of an airline company: Scientific and methodological recommendations]. Orenburg: Orenburg State University. In Russian. [accessed 2023 June 26]. http://elib.osu.ru/bitstream/123456789/10089/1/2101_20110830.pdf

22. Federal State Statistics Service (2023) Regions of Russia. Socio-economic indicators [Internet]. [accessed 2023 June 26] https://rosstat.gov.ru/storage/mediabank/Doklad_2023.htm

23. Shatalova YS (2017) Necessity of External Environmental Analysis of Organisation in the Formation of Competitive Strategy. Acad of Ped Ideas Nov. Ser: Stud Sci Bull 6:1014-1019. In Russian. [accessed 2023 June 26] https://elibrary.ru/item.asp?id=29406422

24. Smirnova EI, Erdnieva AY (2020) Current State and Prospects of The Helicopter Industry in the Russian Federation. Bull Altai Aca Econ Law 11(2):333-339. https://doi.org/10.17513/vaael.1430

25. Sobolev LB (2018) Regional Aviation of Russia. Econ Analys: Theory and Pract 17(1):99-115. https://doi.org/10.24891/ea.17.1.99

26. Tikhonov A (2020) Study of the impact of the life cycle of aircraft engines on the strategy of an engineering enterprise. IOP Conf Ser: Mat Sci and Eng 862(4):042022. https://doi.org/10.1088/1757-899X/862/4/042022

27. Vascik PD, Hansman RJ, Dunn NS (2018) Analysis of Urban Air Mobility Operational Constraints. J Air Transp 26(4):133-146. https://doi.org/10.2514/1.D0120

28. Zhang X, Zhang X (2020) Integrated Requirements Management of Civil Aircraft. IOP Conf Ser: Mat Sci and Eng 751(1):012034. https://doi.org/10.1088/1757-899X/751/1/012034

Maneuvering Star-Convex Extended Target Tracking Based on Modified ExpectedMode Augmentation Algorithm

Jinjin Zhang1, Lifan Sun1,2,* , Dan Gao1
1.Henan University of Science and Technology – School of Information Engineering – Luoyang/Honã – China.
2.Longmen Laboratory – Luoyang – China.Russia

ABSTRACT

In utilizing a variable-structure multiple-model (VSMM) algorithm for kinematic state estimation, the core step is the model set design. This study aims to refine the existing expected-mode augmentation (EMA) algorithm, a method of model set design. First, the OTSU algorithm is employed to determine an adaptive threshold, which in turn allows for a reasonable partition of the basic model set. Next, a subset of possible models is preserved, reactivating models adjacent to the one with the highest prediction probability, eliminating improbable models, and yielding an augmented expected mode. Additionally, the study leverages the translation properties of radial functions and inverse trigonometric function formulas to derive a maneuvering model for starconvex extended targets under uniformly accelerated conditions. In order to assess the effectiveness of the proposed algorithm and the validity of the established maneuvering model, simulation experiments were carried out in both fixed and random scenarios. The proposed algorithm demonstrates improved performance when compared to the interactive multiple-model algorithm and the unmodified EMA algorithm.

Keywords: Extended target tracking; Variable-structure multiple-model; OTSU

INTRODUCTION

This study addresses the tracking problem of extended targets in the context of radar sensors. Extended target tracking can be characterized as the joint estimation of kinematic and extension states. The foundation of any tracking algorithm lies in the tracking models, making the selection of an appropriate model a crucial starting point for subsequent tracking. This paper primarily concentrates on the development of motion models.

Existing single motion models encompass constant acceleration (CA), constant velocity (CV) (Yunita et al. 2020), constant turn (CT) (Amrouche et al. 2018), Singer model (Zhu et al. 2019), Jerk model (Deng et al. 2019), and others. Nonetheless, a single model is often insufficient to describe the complex and variable kinematic behavior of targets in maneuvering scenarios.

When a sudden, intense maneuver occurs, the tracking accuracy may significantly diminish or even result in tracking failure. Subsequently, the interactive multiple-model (IMM) algorithm was proposed for the first time (Blom 1984). This method employs several fixed models for parallel estimation at each instance, while concurrently introducing interaction among these models (Qu et al. 2009). Ultimately,

the estimation results of each model are fused based on updated model probabilities.

However, this approach can only achieve optimal estimation when the model set corresponds to the true pattern. In an attempt to maximize the approximation to the target's true motion mode, it is common to increase the number of models. Nevertheless, this not only escalates the computational burden but may also lead to reduced tracking accuracy due to competition between models (Shen-tu et al. 2018).

To overcome this predicament, there are two potential solutions: either develop a superior model set or employ a variable model set. Li and Bar-Shalom (1996) initially introduced a variable-structure multiple-model (VSMM) algorithm. In comparison to the fixed-structure multi-model (FSMM) algorithm, the VSMM algorithm includes model set design, which can also be perceived as a model-set adaptation (MSA) module. This module can determine which models from the entire set will be chosen to carry out subsequent multiple-model (MM) estimation operations at each instance. As a result, a smaller number of models can achieve a higher degree of approximation to the true system mode. The one-time recursive process of the VSMM algorithm accomplishes two primary tasks, which can be summarized as follows:

• MSA: Tasked with utilizing prior and posterior information to determine the model set at each instance, primarily focusing on activating new models and terminating a subset of the current model set (Lan and Li 2013). The objective of activating a new model is to identify a "superior" model, which is incorporated into the existing model set and then utilized collectively for state estimation. In this context, "superior" implies that the newly activated model can more accurately describe the true system mode. Conversely, the goal of terminating a model is to eliminate models that significantly deviate from the system mode; thus, reducing computational demands while avoiding unnecessary competition between models.

• VSIMM (Shen et al. 2021): Responsible for estimating the target state using the IMM approach under the condition of a given model set.The distinction between various VSMM algorithms lies in the differing model-set adaptation strategies. The expected mode augmentation (EMA) algorithm is classified as a model activation method (Li et al. 2005). While maintaining the basic model set, it extends an expected mode, which is the probability-weighted sum of the basic model. Figure 1 presents valid model topology diagrams for 7, 9, and 13 basic models, with different coordinate positions corresponding to varying levels of maneuver. The tracking performance of the EMA algorithm is significantly superior to that of the IMM algorithm. However, its basic model set is predefined and unchangeable, leading to limited adaptability of the augmented expected mode to the basic model set. Ideally, the model should adapt in real time based on the potential kinematic behavior of the target.

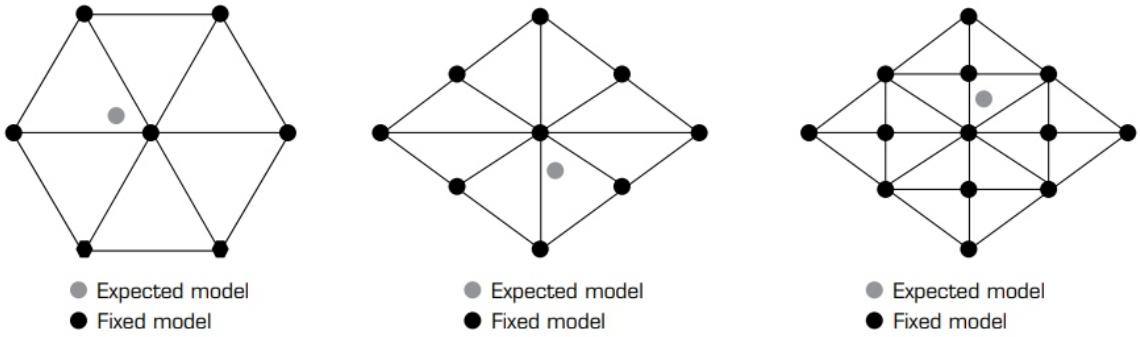

Source: Adapted from Li et al. (2005).

Figure 1. The model topological structure diagram of EMA algorithm.

The likely-model set (LMS) algorithm (Li and Zhang 2000) divides the original model set into unlikely model sets ML k-1, general model sets MMk-1, and important model sets MHk-1 by setting threshold values based on the model probability when determining the model set Mk at k. Subsequently, it discards the unlikely models with low probability while retaining the general and crucial models. Besides, if there are important models (m(I) | m(I) ϵ MHk-1), activate the model set Am(i) adjacent to them to obtain the changed model group Mk. The adaptive strategy of LMS can be represented by the Eq. 1:

$$M_k = \left(M_{k-1} - M_{k-1}^L\right) \cup \left(\bigcup_{m^{(i)} \in M_{k-1}^H} A_{m^{(i)}} \right) \quad (1)$$

where Mk-1 represents the valid set of models at k-1.

The LMS algorithm can maintain estimation accuracy while reducing a certain amount of computation. However, it is unable to activate models outside the comprehensive model set, leading to higher peak errors during target maneuvers. Moreover, fixed thresholds are employed when determining different subsets of models.

The fixed threshold method demonstrates effective clustering for model sets with substantial probability differences among various models, facilitating the division of each model subset. Conversely, when probabilities between models are closely related, assessing their relative importance becomes challenging. The OTSU algorithm incorporates clustering concepts, enabling the identification of an appropriate numerical level through variance calculations to bifurcate the elements within the entire numerical set, maximizing the overall numerical value difference between the two parts and minimizing the difference within each part (Otsu 1979; Qian et al. 2021; Xiao et al. 2022; Zhao 2022). Consequently, the OTSU algorithm can be utilized for clustering numeric sets.

Inspired by the design idea of the LMS algorithm, this study introduces a novel model set design method based on EMA, ingeniously employing OTSU. Initially, the OTSU algorithm is utilized to

automatically select a threshold value at any given time, enabling the binarization of the model prediction probability set. Then, the minimum value in the large category is taken as the threshold value for "retaining models" and "eliminating models" to obtain two different subsets of models (likely subset $M_l = \bigcup \left(m_{k-1}^i \mid \mu_{k|k-1}^i \geq \tau \right)$ and unlikely subset $M_u = \bigcup \left(m_{k-1}^i \mid \mu_{k|k-1}^i < \tau \right)$). Meanwhile, the model adjacent to the most likely model $m_{k-1}^s \mid \mu_{k|k-1}^s = \max\left(\mu_{k|k-1} \right)$ is reactivated. Thus, the basic model set at k can be determined.

Finally, an augmented model is acquired based on the prediction probability and parameters of the preserved basic model. Additionally, a maneuvering model for star-convex extended targets under uniformly accelerated scenarios is derived, enabling the joint estimation of kinematic and extension states. In order to validate the effectiveness of the proposed algorithm, simulation experiments were performed in both deterministic and random scenarios. When compared to the fixed IMM and original EMA algorithm, the proposed algorithm demonstrates a notable enhancement in tracking speed and accuracy.

PROBLEM FORMULATION

State equation

The transition process between states can be modeled as a simple stochastic hybrid system, i.e., a linear time-varying system (Eq. 2).

$$\begin{bmatrix} x_k^m \\ x_k^e \end{bmatrix} = \begin{bmatrix} F_k^m & 0 \\ 0 & F_k^e \end{bmatrix} \begin{bmatrix} x_{k-1}^m \\ x_{k-1}^e \end{bmatrix} + \begin{bmatrix} w_k^m \\ w_k^e \end{bmatrix}, k \in \mathrm{N} \tag{2}$$

where xmk and xek denote kinematic and morphological parameter vectors, Fmk and Fek are corresponding state transition matrices. wmkand wek are uncorrelated process noise sequences.

Measurement equation

The measurement generation process of star-convex extended targets includes the establishment of measurement source model and sensor model, as shown in Fig. 2. For an extended target, since measurement data sources may also be distributed inside the boundary, scaling the boundary can be selected to cover its internal situation (Zhang et al. 2022). For an unknown measurement source data y(l)k, if a matching scaling factor Ŝk (Ŝk ∈ [0,1]) is known, its location can be defined by Eq. 3:

$$y_k^{(l)} \in x_k^c + \hat{s}_k (S(x_k) - x_k^c) \tag{3}$$

where xCk denotes the centroid position, and S(xk) represents the contour point.

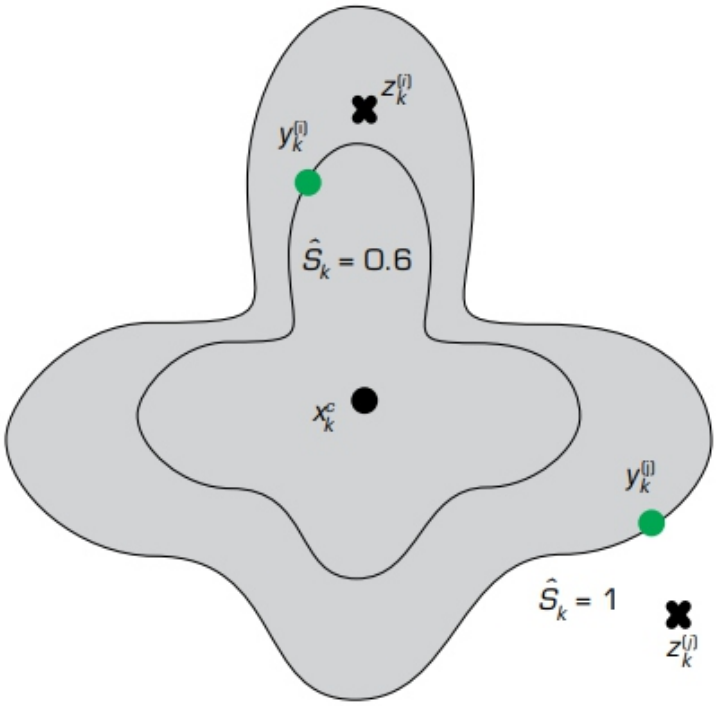

Source: Elaborated by the authors.

Figure 2. Measurement model for extended targets: Independent generation of measurements.

Furthermore, for a given single measurement data source y (l)k, the sensor model defines the measurement location by Eq. 4

$$z_k^{(l)} = y_k^{(l)} + v_k \qquad (4)$$

where z(l)k is the lth measurement data, and vk represents Gaussian white noise with a zero-mean value. The measurement generation process of the extended target is shown in Fig. 3, which can be summarized as an extent source model and a sensor model.

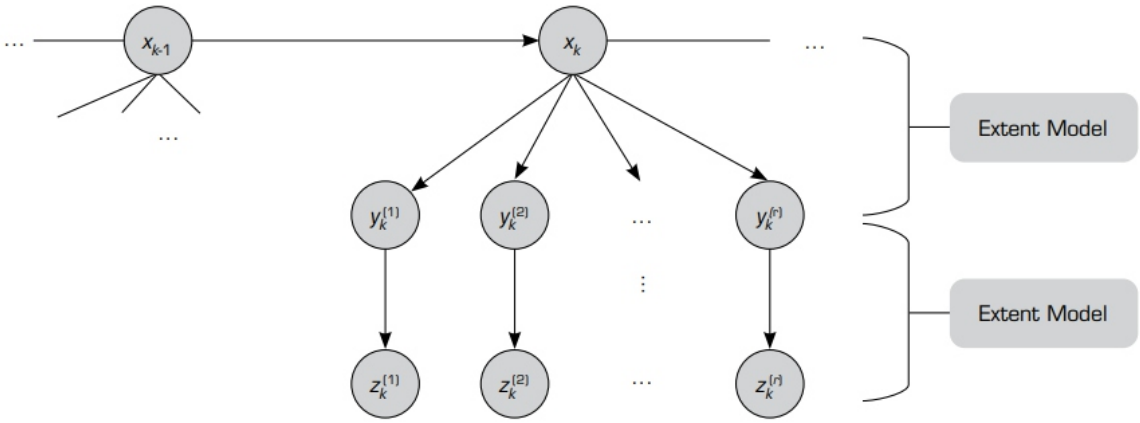

Source: Retrieved from Baum (2013).

Figure 3. Measurement generation process for extended targets (visualization).

Model jump equation

The jump process between models can be considered as a first order Markov chain, and the transition probability can be defined by Eq. 5:

$$P\{s_k = m_j | s_{k-1} = m_i\} = \pi_{ij}, \forall m_i, m_j \in M \quad (5)$$

where the set M contains all the possible motion models of the system, πij represents the transition probability from state mi to mj. Figure 4 shows the structural diagram of the transition between states in a Markov chain.

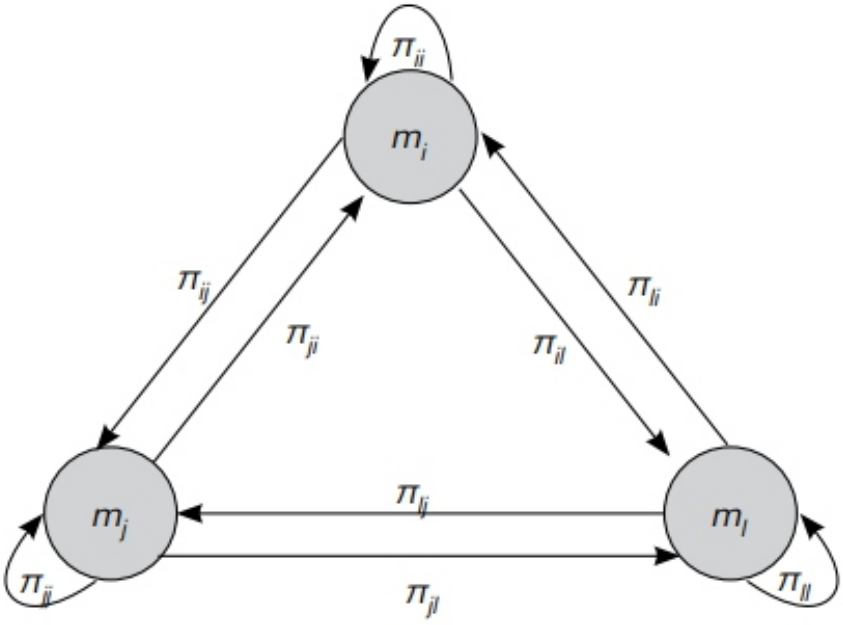

Source: Elaborated by the authors.

Figure 4. State transition diagram of Markov chain.

THE PROPOSED MEMA ALGORITHM

S1. Model set partitioning: Divide the basic model set Mb k-1 at k-1 into likely model subset $M_l (M_l = \bigcup_{i=1}^{p} (m_{k-1}^i \mid \mu_{k|k-1}^i \geq \tau))$ and unlikely model subse $M_u (M_u = \bigcup_{i=1}^{q} (m_{k-1}^i \mid \mu_{k|k-1}^i < \tau))$. Here, the threshold value τ can be adaptive according to the OTSU algorithm, which uses variance calculations to find an appropriate numerical level τ to divide the elements of the entire set (Mbk-1; m1, m2, ..., mr) into two subsets Ml and Mu. The partitioning process maximizes the difference between the overall values (i.e., model prediction probability μik|k-1)in the two subsets, and minimizes the difference between the values in each subset. The specific division process is as the following:Assuming that the number of models in the basic model set Mbk-1 is r, the proportion of the number of models in Ml to the total

$$\lambda_1 = \frac{p}{r}, \quad \lambda_o = \frac{q}{r}, \quad \lambda_1 + \lambda_0 = 1 \tag{6}$$

$$\lambda_1\rho_1 + \lambda_0\rho_0 = 1 \tag{7}$$

$$g = \lambda_1\lambda_0 * (\lambda_1 - \lambda_0)^2 \tag{8}$$

Then, using the traversal method to obtain a threshold value τ that maximizes the inter class variance. The reasons why using OTSU algorithm for model set partitioning can be summarized as follows:

• The calculation is simple, and the model set can also be effectively divided when the numerical values of the model probabilities in the set do not differ significantly;

• Compared to the method of using a fixed threshold for partitioning, it can achieve adaptation based on the distribution of elements in the set, making the partitioning process more reasonable.

S2. Model-set adaptation: Calculate Mk according to Mk = Mbk U Ek, where Mk defines the set of all possible models at k,Mbkcontains models in the basic model set, and Ek is the augmented expected mode. Specifically, it contains the following four steps:

• Retention of likely models: Retain all models in the subset Ml.

• Activation of a new model: Activates the model set Ma adjacent to the most likely model (msk-1|μsk|k-1 = max (μk|k-1)).

• Elimination of unlikely models: Delete all models that are not activated in the unlikely model set Mu, then the basic model set at k is Mbk = Mbk-1 – (Mu – Mu ∩ Ma).

• Augmentation of expected mode: Use the newly generated basic model set Mbk and its prediction probability μik|k-1 to obtain an augmented expected mode Ek = E(Mbk; m1, m2, ... me). where e is the number of models in the basic model set Mbk.

The entire process of the proposed MEMA algorithm can be briefly described in Table 1.

Table 1. The proposed MEMA algorithm.

Step	Title	Description
1	Initialization	a) Design total model set $\{M_{k\text{-}1}\}$; b) Design basic model set $\{M^b_{k\text{-}1}\}$;
2	Model set partitioning	a) Calculate threshold τ using OTSU; b) Likely models, $M_l = U^p_{i=1}\{m^i_{k\text{-}1} \mid \mu^i_{k\mid k\text{-}1} \geq \tau\}$; c) Unlikely models, $M_u = U^q_{i=1}\{m^i_{k\text{-}1} \mid \mu^i_{k\mid k\text{-}1} < \tau\}$;
3	Model-set adaption	a) Retain all the models in M_l; b) Activate the models M_a adjacent to the most likely model; c) Delete the inactive model in M_u; d) Obtain the basic model set according to $M^b_k = M^b_{k\text{-}1} - \{M_u - M_u \cap M_a\}$ and calculate E_k; e) Determine the current total model set according to $M_k = M^b_k \cup E_k$;
4	Model-set sequence conditioned estimation	Run VSIMM;
5	Send output	$\{\hat{x}_i(k\mid k), P_i(k\mid k), \mu_i(k)\}\ m_i \in M_k$

Source: Elaborated by the authors.

A MANEUVERING MODEL FOR STAR-CONVEX EXTENDED TARGET UNDER UNIFORM ACCELERATION SCENARIO

The state of the extended target includes dynamic and morphological variables, and there is a coupling relationship between them (Baum 2013; Liu et al. 2022). For example, when a target generates maneuvers such as constant acceleration, it is necessary to ensure that the orientation of shape is always consistent with the direction of movement. Therefore, how to establish a concise maneuver model to simultaneously describe the dynamic evolution process of two variables is a key issue to be solved in extended target tracking. In this paper, using the translation characteristics of radial function and the inverse trigonometric function formula, the morphological evolution equation of a star-convex maneuvering extended target in a uniform acceleration scenario is derived. Furthermore, combined with the dynamic equation of kinematic state, a complete maneuvering model is obtained. The content of this chapter is the preparatory work for the subsequent simulation.

As shown in Fig. 5, the contour of a star-convex extended target can be described using a radial function in the two-dimensional coordinate system.

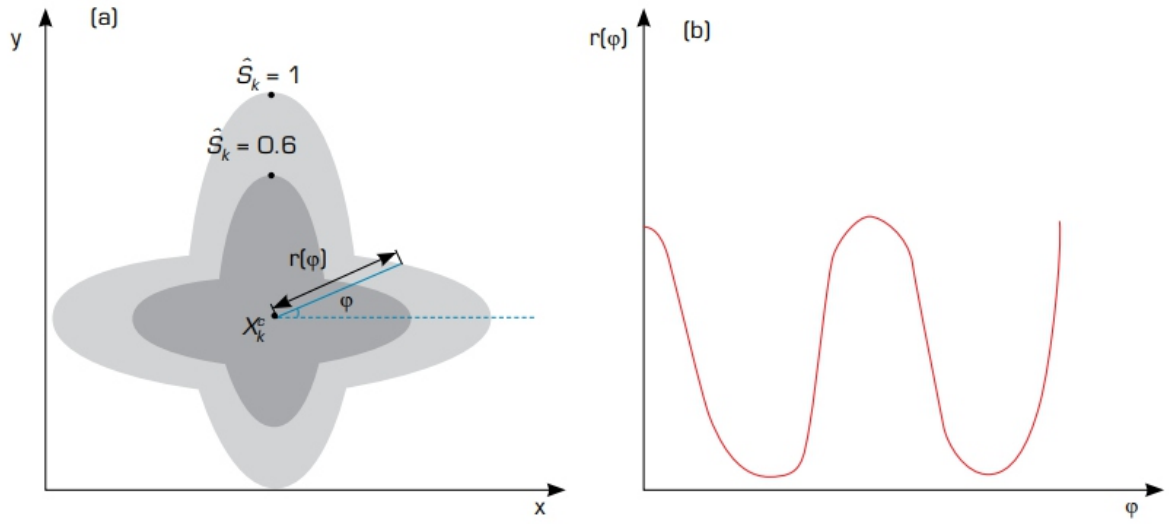

Source: Elaborated by the authors.

Figure 5. Representing a star-convex shape with the radial function. (a) Star-convex target; (b) Radial function.

The horizontal axis ranges from 0 to 2π, and the size of the vertical axis defines the distance between each contour point and the centroid xck. The contour _S(xk) after zooming can be described as follows (Eqs. 9 and 10) (Baum and Hanebeck 2014):

$$\bar{S}(x_k) = \{\hat{s}_k r(\varphi) e(\varphi) + x_k^c | \varphi \in [0,2\pi), \hat{s}_k \in [0,1]\} \quad (9)$$

$$e(\varphi) = \begin{bmatrix} \cos(\varphi) \\ \sin(\varphi) \end{bmatrix} \quad (10)$$

Perform a linearization process on the radial function, i.e., Fourier series expansion (Eqs. 11–13),

$$r(B_k, \varphi) = a_k^{(0)} + \sum_{j=1,\cdots,N^F} \left(a_k^{(j)} \cos(j\varphi) + b_k^{(j)} \sin(j\varphi) \right) = R(\varphi) B_k \quad (11)$$

$$R(\varphi) = \left[1, \cos(\varphi), \sin(\varphi), \ldots, \cos\left(N^F \varphi\right), \sin\left(N^F \varphi\right) \right] \quad (12)$$

$$B_k = \left[a_k^{(0)}, a_k^{(1)}, b_k^{(1)}, \ldots, a_k^{\left(N^F\right)}, b_k^{\left(N^F\right)} \right]^T \quad (13)$$

where NF represents the order of Fourier expansion. The higher the order, the more detailed morphological information can be reflected by its coefficients. The extension parameter vector xek can be represented by Bk, Eq. 14:

$$x_k^e = \left[a_k^{(0)}, a_k^{(1)}, b_k^{(1)}, \ldots, a_k^{\left(N^F\right)}, b_k^{\left(N^F\right)} \right]^T \quad (14)$$

The radial function has a translational characteristic. When the target rotates angle θ, the radial function also shifts the corresponding angle in the horizontal direction. According to this property, the radial function after rotation can be obtained through translation calculation based on the radial function at the previous moment, Eq. 15:

$$r(x_k^e, \varphi) = r(x_{k-1}^e, \varphi - \theta) + w_{k-1}^e \quad (15)$$

Literature (Sun et al. 2021) has derived the maneuvering model of a star-convex extended target in a turning scenario, Eqs. 16–19:

$$\begin{bmatrix} x_k^m \\ x_k^e \end{bmatrix} = \begin{bmatrix} F_k^m(\theta) & 0 \\ 0 & F_k^e(\theta) \end{bmatrix} \begin{bmatrix} x_{k-1}^m \\ x_{k-1}^e \end{bmatrix} + \begin{bmatrix} w_k^m \\ w_k^e \end{bmatrix}, k \in \mathrm{N} \quad (16)$$

$$F_k^m(\theta) = \begin{bmatrix} 1 & \frac{\sin\theta}{\omega} & 0 & \frac{\cos\theta}{w} \\ 0 & \cos\theta & 0 & -\sin\theta \\ 0 & \frac{1-\cos\theta}{\omega} & 1 & \frac{\sin\theta}{\omega} \\ 0 & \sin\theta & 0 & \cos\theta \end{bmatrix} \quad (17)$$

$$F_k^e(\theta) = diag\left(1, F^{e,1}, \cdots, F^{e,N_F}\right) \tag{18}$$

$$F^{e,j} = \begin{bmatrix} \cos(j\theta) & -\sin(j\theta) \\ \sin(j\theta) & \cos(j\theta) \end{bmatrix}, j = 1, \cdots N_F \tag{19}$$

If a target undergoes a motion of constant acceleration, its kinematic state can be defined as xm k = (xk, vk(x), ak(x), yk, vk(y), ak(y))T,where (ak(x), ak(y))T represents the acceleration vector, ak(x) and ak(y) define the acceleration on the horizontal and vertical axes, respectively. Combined with the inverse trigonometric function formula, it can be deduced that (Eq. 20):

$$\theta = \arccos\left(\frac{v_{k(x)}}{\sqrt{\left(v_{k(x)}\right)^2 + \left(v_{k(y)}\right)^2}}\right) \tag{20}$$

Substituting the above into Eqs. 18 and 19 to obtain the transition matrix of extension parameter, i.e., Fe k (ak(x), ak(y)). The transition matrix of kinematic parameter is (Eq. 21):

$$F_k^m\left(a_{k(x)}, a_{k(y)}\right) = \begin{bmatrix} 1 & T & \frac{T^2}{2} & 0 & 0 & 0 \\ 0 & 1 & T & 0 & 0 & 0 \\ 0 & 0 & 1 & 0 & 0 & 0 \\ 0 & 0 & 0 & 1 & T & \frac{T^2}{2} \\ 0 & 0 & 0 & 0 & 1 & T \\ 0 & 0 & 0 & 0 & 0 & 1 \end{bmatrix} \tag{21}$$

By substituting Fek(ak(x), ak(y)) and F mk(ak(x), ak(y)) into Eq. 2, the dynamic equation of a star-convex extended target in uniform acceleration motion can be obtained.

SIMULATION RESULTS AND DISCUSSIONS

To test the effectiveness of the proposed MEMA algorithm and validate the established maneuver model, the experiment will be conducted through Monte Carlo simulation under a constant acceleration scenario. The tracking object is a single maneuvering extended target, which does not involve clutter and missed detection issues. Besides, in order to reflect fairness, a deterministic scenario (DS) and a random scenario (RS) are set respectively.

Deterministic scenario (DS)

The simulation was conducted in a constant accelerated scenario, and the algorithms involved in the comparison were the IMM and EMA algorithms. Root-mean-square-error (RMSE) and Hausdorff distance (Marošević 2018) are used to evaluate the estimation accuracy of motion state and shape, respectively. The smaller the value, the higher the accuracy.The total number of models in the IMM algorithm is 7, and the number of basic model sets both in EMA and MEMA is also uniformly set to 7. Specific parameters can be defined by Eq. 22.

$$\left\{a_1 = (0,0)^T\ a_2 = (20,0)^T\ a_3 = \left(10,10\sqrt{3}\right)^T\ a_4 = \left(-10,10\sqrt{3}\right)^T\ a_5 = (-20,0)^T\ a_6 = \left(-10,-10\sqrt{3}\right)\ a_7 = \left(10,-10\sqrt{3}\right)^T\right\} \quad (22)$$

The initial kinematic state of the target is xmo = (1000,0, - 10,5000, - 200, -10)T. Table 2 shows the detailed maneuvering process.

The program performs 100 simulation steps each time, during which the acceleration (m/s2)of the target changes a total of 4 times.

Table 2. Maneuvering process in DS.

Step	[0,20]	[20,40]	[40,60]	[60,80]	[80,100]
Acceleration	(3,3)	(-2,-2)	(3,3)	(-3,-3)	(3,3)

Source: Elaborated by the authors.

Figure 6, Tables 3 and 4 show the overall performance evaluation results of the three algorithms. Compared to the fixed IMM algorithm, EMA and MEMA perform better in both kinematic and extension parameters estimation. This can be attributed to a time-varying set of models based on the possible motion patterns of the target. In other words, the augmented expected mode can better match the true system mode to some extent. Therefore, even if the target maneuvers, there will not be a significant peak error. Furthermore, compared to EMA, MEMA exhibits higher estimation accuracy and less computational complexity. The reasons may be summarized as follows: On the one hand, the MEMA algorithm sets the basic model set to be variable, eliminating mismatched models at every moment, thus reducing unnecessary competition between models. On the other hand, using variable thresholds for model set partitioning enhances the rationality and fairness of the partitioning process.

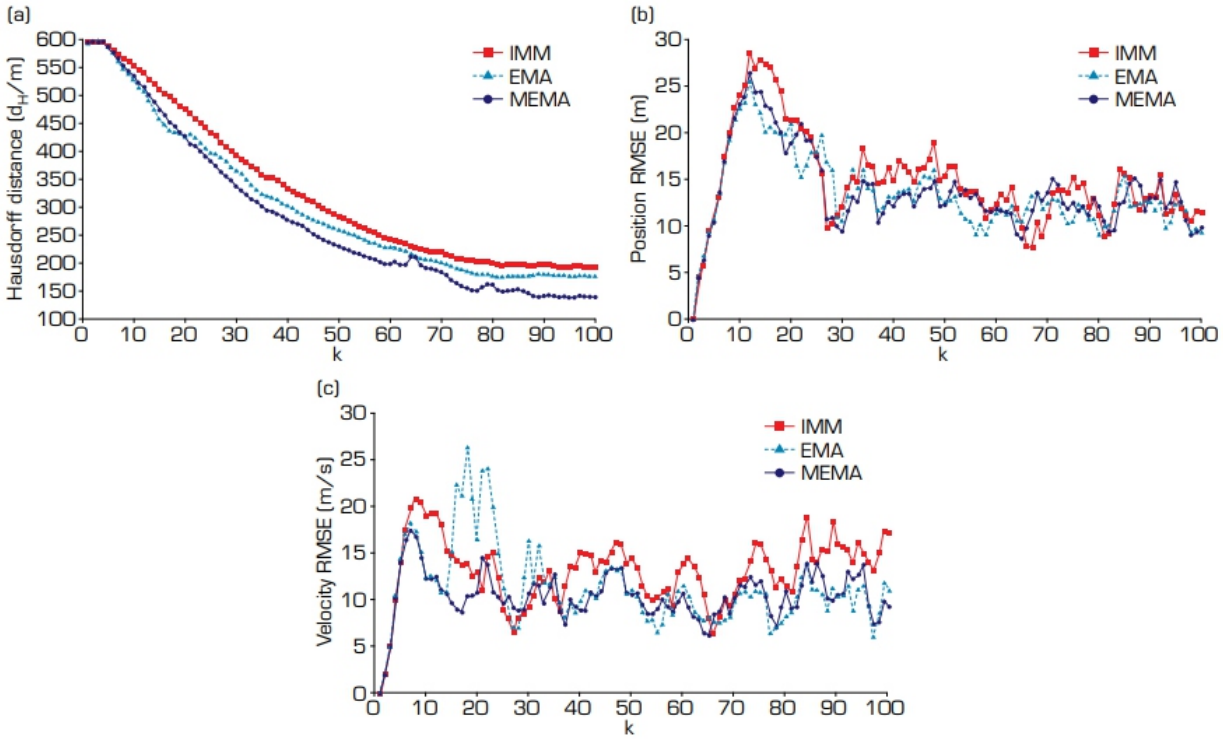

Source: Elaborated by the authors.

Figure 6. Performance comparisons of the three algorithms in DS. (a) Hausdorff distance; (b) Position RMSE; (c) Velocity RMSE.

Table 3. Performance comparisons of the three algorithms in DS.

	Hausdorff distance (d_H/m)	Position RMSE (m)	Velocity RMSE (m/s)
IMM	327.172	14.912	13.040
EMA	303.045	13.570	11.324
MEMA	283.183	13.748	10.375

Source: Elaborated by the authors.

Table 4. Single run time of three algorithms in DS.

Algorithm	IMM	EMA	MEMA
Time (s)	3.139	3.677	3.361

Source: Elaborated by the authors.

Random scenario (RS)

In order to provide a relatively fair testing environment, another simulation scenario is set up. In this scenario, the acceleration of the target in both the horizontal and vertical directions is random, and the time τT spent at a certain acceleration is also random. Relevant parameters are set as follows:

The acceleration in the horizontal direction is defined as ax = amax * cosβ, and that in the numerical direction is ay = amax * sinβ.where amax = 10√_

2, β ϵ (0°, 135°), five β within the range of this angle during a single program execution will be randomly generated. The simulation program executes 50 steps each time, and the residence time τt corresponding to a certain acceleration (ax, ay) is a random number that satisfies the condition .

Figure 7, Tables 5 and 6 show the performance comparison results of the three algorithms. Hausdorff distance is an indicator used to measure the performance of morphological estimation during extended target tracking. The smaller the value, the closer the estimated result of the corresponding algorithm is to the true shape. Velocity and position RMSE can judge the accuracy of tracking algorithms in estimating motion behavior (including position, velocity, etc.). Similarly, the smaller the value, the better the performance. In this simulation scenario, the maneuvering behavior of the target at each moment is random, which poses a high challenge to the tracking algorithm. Compared to the EMA algorithm, the proposed MEMA algorithm improves tracking accuracy while also reducing a certain amount of computation. Moreover, the performance of the MEMA algorithm in the entire tracking process has been relatively stable compared to the other two algorithms, indicating that the robustness of MEMA is better.

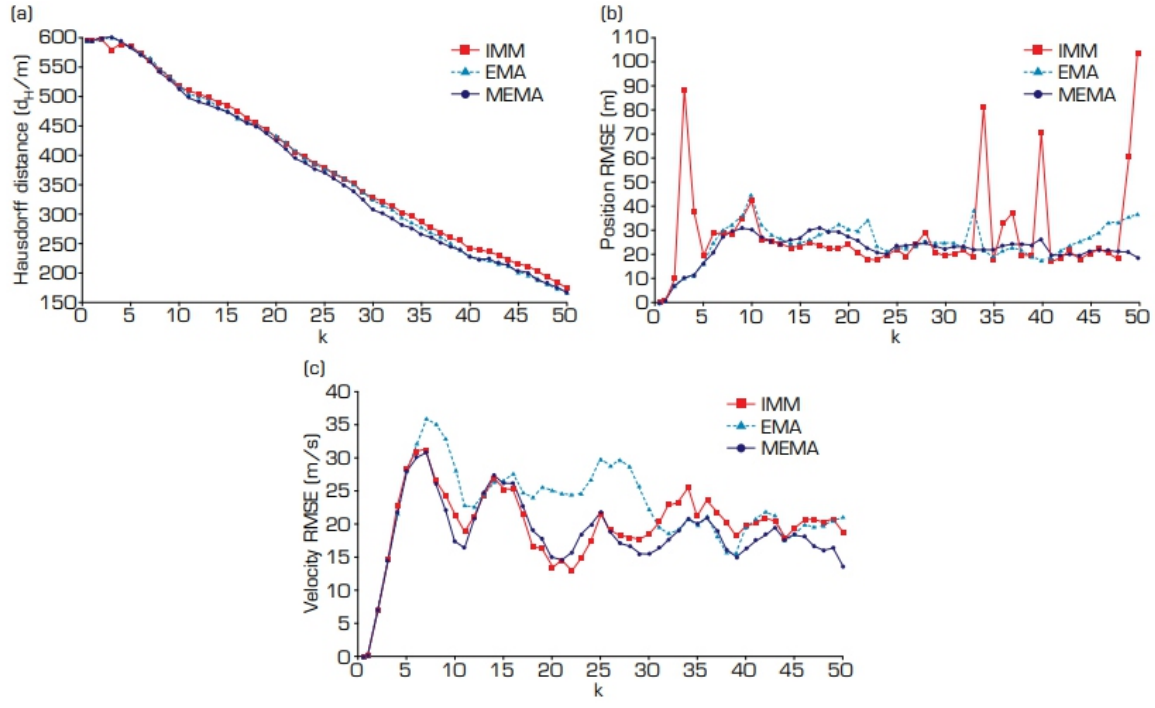

Source: Elaborated by the authors.

Figure 7. Performance comparisons of the three algorithms in RS.

(a) Hausdorff distance; (b) Position RMSE; (c) Velocity RMSE.

Table 5. Performance comparisons of the three algorithms in RS

	Hausdorff distance (d_H/m)	Position RMSE (m)	Velocity RMSE (m/s)
IMM	381.515	28.999	21.254
EMA	376.107	24.817	23.058
MEMA	371.506	23.965	20.181

Source: Elaborated by the authors.

Table 6. Single run time of three algorithms in RS.

Algorithm	IMM	EMA	MEMA
Time (s)	1.729	1.964	1.931

Source: Elaborated by the authors.

DISCUSSION

In the two simulation scenarios established in this study, the overall performance of the MEMA algorithm surpasses that of the IMM and EMA, attributable to three inherent characteristics of the algorithm:• Utilizing the OTSU algorithm, a variable threshold value is computed based on the model's prediction probability, enabling a reasonable partitioning of the existing basic model set;• Activation and termination strategies for the model are provided, eliminating some implausible models and retaining only potential matching models, resulting in a relatively reduced computational burden;

• By anticipating the possible movement trends of the target and reactivating more suitable models, the algorithm can better adapt to state changes.

CONCLUSION

This paper investigates the existing VSMM framework and introduces a novel model-set design method based on the EMA algorithm. On the one hand, through model set partitioning, some implausible models in the basic model set are removed, thus, reducing unnecessary competition between models. On the other hand, by utilizing the OTSU algorithm to obtain variable thresholds during model set partitioning, the irrationality and limitations of previously fixed thresholds are effectively circumvented. Moreover, a maneuvering model for star-convex extended targets in a uniform acceleration scenario is constructed, employing the translational invariance of radial functions and the inverse cosine function formula. Simulation experiments in fixed and random scenarios further substantiate that the proposed algorithm can efficiently enhance the tracking performance of targets in maneuvering scenarios.

CONFLICT OF INTEREST

Nothing to declare.

AUTHOR CONTRIBUTIONS

Conceptualization: Zhang J; Data curation: Zhang J and Sun L; Formal analysis: Sun L; Acquisition of funding: Sun L;Research: Zhang J and Sun L; Methodology: Zhang J; Project administration: Sun L and Gao D; Resources: Sun L and Gao D;Software: Zhang J and Sun L; Supervision: Sun L and Gao D;Validation: Zhang J and Sun L; Writing - Preparation of original draft: Zhang J and Sun L; Writing - Proofreading and editing: Zhang J and Sun L.

FUNDING

Aeronautical Science Foundation of China
https://doi.org/10.13039/501100004750
Grant No: 20185142003

Major Science and Technology Projects of Longmen Laboratory
Grant No: 231100220200
National Natural Science Foundation of China
https://doi.org/10.13039/501100001809
Grant No: 62271193
Natural Science Foundation of Henan Province
https://doi.org/10.13039/501100006407
Grant No: 222300420433
Science and Technology Innovative Talents in Universities of Henan Province
Grant No: 21HASTIT030
Young Backbone Teachers in Universities of Henan Province
Grant No: 2020GGJS073

ACKNOWLEDGMENTS

Not applicable.

REFERENCES

1. Amrouche N, Khenchaf A, Berkani D (2018) Detection and Tracking Low Maneuvering Target in a High Noise Environments. Paper presented at 2018 International Conference on Radar (RADAR). IEEE; Brisbane, Australia. https://doi.org/10.1109/RADAR.2018.8557244

2. Baum M (2013) Simultaneous Tracking and Shape Estimation of Extended Objects (doctoral

dissertation). Karlsruhe: Karlsruhe Institute of Technology.

3. Baum M, Hanebeck UD (2014) Extended Object Tracking with Random Hypersurface Models. IEEE Trans Aerosp Electron Syst 50(1):149-159. https://doi.org/10.1109/TAES.2013.120107

4. Blom HAP (1984) An Efficient Filter for Abruptly Changing Systems. Paper presented at The 23rd IEEE Conference on Decision and Control. IEEE; Las Vegas United States. https://doi.org/10.1109/CDC.1984.272089

5. Deng Q, Chen G, Lu H (2019) Adaptive Sample-Size Unscented Particle Filter with Partitioned Sampling for Three Dimensional High-Maneuvering Target Tracking. Appl Sci 9(20):4278. https://doi.org/10.3390/app9204278

6. Lan J, Li X-R (2013) Equivalent-model Augmentation for Variable-structure Multiple-model Estimation. IEEE Trans Aerosp Electron Syst 49(4):2615-2630. https://doi.org/10.1109/TAES.2013.6621840

7. Li X-R, Bar-Shalom Y (1996) Multiple-model estimation with variable structure. IEEE Trans Autom Control 41(4):478-493. https://doi.org/10.1109/9.489270

8. Li X-R, Zhang Y (2000) Multiple-Model Estimation with Variable Structure Part V: Likely-Model Set Algorithm. IEEE Trans Aerosp Electron Syst 36(2):448-466. https://doi.org/10.1109/7.845222

9. Li X-R, Jilkov VP, Ru J (2005) Multiple-model Estimation with Variable Structure-part VI: Expected-mode Augmentation. IEEE Trans Aerosp Electron Syst 41(3):853-867. https://doi.org/10.1109/TAES.2005.1541435

10. Liu S, Xue M, Qiu Y, Zhou X, Zhao Q (2022) Design of the Missile Attitude Controller Based on the Active Disturbance Rejection Control. J Aerosp Technol Manag 14:e1322. https://doi.org/10.1590/jatm.v14.1255

11. Marošević T (2018) The Hausdorff distance between some sets of points. Math Commun 23(2):247-257. https://hrcak.srce.hr/198692

12. Otsu N (1979) A Threshold Selection Method from Gray-level Histograms. IEEE Trans Syst Man Cybern 9(1):62-66. https://doi.org/10.1109/TSMC.1979.4310076

13. Qian F, Lei H (2021) A pupil location algorithm based on cascaded Haar feature and OTSU dynamic threshold segmentation. Paper presented at AOPC 2021: Optical Sensing and Imaging Technology (Vol. 12065, pp. 796-801). SPIE; Beijing, China. https://doi.org/10.1117/12.2607002

14. Qu HQ, Pang LP, Li SH (2009) A novel interacting multiple model algorithm. Signal Processing 89(11):2171-2177. https://doi.org/10.1016/j.sigpro.2009.04.033

15. Shen N, Chen L, Lu X, Hu H, Pan Y, Gao Z, Liu X, Liu Z, Chen R (2021) Online Displacement Extraction and Vibration Detection Based on Interactive Multiple Model Algorithm. Mech Syst Signal Process 155:107581. https://doi.org/10.1016/j.ymssp.2020.107581

16. Shen-tu H, Luo J-a, Xue A, Peng D, Guo Y (2018) A Novel Variable Structure Multi-Model Tracking

Algorithm Based on Error-Ambiguity Decomposition. Paper presented at 2018 21st International Conference on Information Fusion (FUSION). IEEE; Cambridge, United Kingdom. https://doi.org/10.23919/ICIF.2018.8455416

17. Sun L, Yu H, Fu Z, He Z, Zou J (2021) Modeling and Tracking of Maneuvering Extended Object with Random Hypersurface. IEEE Sens J 21(18):20552-20562. https://doi.org/10.1109/JSEN.2021.3097967

18. Xiao J, Li H, Jin H (2022) Transtrack: Online Meta-Transfer Learning and OTSU Segmentation Enabled Wireless Gesture Tracking. Pattern Recognit 121:108157. https://doi.org/10.1016/j.patcog.2021.108157

19. Yunita M, Suryana J, Izzuddin A (2020) Error Performance Analysis of IMM-Kalman Filter for Maneuvering Target Tracking Application. Paper presented at 2020 6th International Conference on Wireless and Telematics (ICWT). IEEE; Yogyakarta, Indonesia. https://doi.org/10.1109/ICWT50448.2020.9243662

20. Zhang X, Yan Z, Chen Y, Yuan Y (2022) A novel particle filter for extended target tracking with random hypersurface model. Appl Math Comput 425:127081. https://doi.org/10.1016/j.amc.2022.127081

21. Zhao L (2022) Motion Track Enhancement Method of Sports Video Image Based on OTSU Algorithm. Wirel Commun Mob Comput 2022:8354075. https://doi.org/10.1155/2022/8354075

22. Zhu M, Yu F, Xiao S (2019) An Unconventional Multiple Low-Cost IMU and GPS-Integrated Kinematic Positioning and Navigation Method Based on Singer Model. Sensors 19(19):4274. https://doi.org/10.3390/s19194274

Investigating the Effect of Applying Uniform Distributed Load on the De!ection of Simply Supported Axial - Functionally Graded Beam

Zainab M Shukur1,* , Raisan Faris Hamad1 , Yassar Khadhim Ali1 , Luay Sadiq Al-Ansari1 , Mohammedh Helayel Al-Karaishi

.University of Kufa – Faculty of Engineering – Department of Mechanical Engineering – Najaf – Iraq.

A B S T R A C T

Axially-functionally graded materials are/ types of traditional composite materials in which the mechanical and physical properties are gradually varied from one end to the other. !ey were used extensively in industries such as defense, automotive and aerospace because of the ability to design its mechanical and physical properties. Two numerical models are built in this work in order to investigate the de"ection of a simply supported beam made by axial-functionally graded material. !e #rst model is the new model and it is built by adopting the Rayleigh Method, while the second model used the Finite-Element technique to build an 1D model utilizing the ANSYS APDL. !e mechanical and physical of the axial-functionally graded beam were changed in axial direction according to Power-Law Equation. !e new model, based on Rayleigh Method ANSYS- 1D model, shows an excellent agreement with the results and available literature. In addition to the validation of the two models, the in"uences of elastic moduli ratio and material distribution on the maximum static de"ection and its position were studied. In ANSYS- 1D model, the position of the maximum de"ection was deviated from the middle span of A-FG beam and this deviation in position of maximum de"ection reduces, as well as increases the index of power-law equation and the elastic moduli ratio (ME-Ratio) when it diverges from 1.

Keywords: Axially-functionally graded beam; Power-law equation; Uniform distributed load; Simply supported beam.

I. INTRODUCTION

In mechanical and structural applications, metals (Kassner et al. 2015), alloys (Saleh et al. 2021; Xu et al. 2019), ceramics (Ashby 2000; Majeed et al. 2017; Shao 2018), polymers (Kalyanet al. 2017; Osswald et al. 2010), and conventional composites (i.e., chopped-#ber composites, longitudinal-#ber composites and laminated composites) (Harris 1999; Kaw 2006; Xu et al. 2020), were manufactured to get homogenous properties (Saleh et al. 2020b). Sometimes these materials cannot meet the requirements of engineering applications because of limitations of their material properties (Saleh et al. 2019; Fathi et al. 2020). !erefore, it was essential to enhance mechanical and physical properties to achieve the requirements of engineering applications (El-Galy et al.2018) by manufacturing a new material, called “Functionally Graded Materials (FGMs)”. !e FGM can be de#ned as “Functionally Grade Materials (FGMs) are kind of composite materials in which the material properties are designed

to vary continuously and gradually from one surface to the other in order to eliminate the discontinuity e$ects in properties" (Bhavar et al. 2017; Ebhota and Jen 2018; Helal 2020; Jamian 2012; Walaa 2021); or "Functionally graded materials (FGMs) are a broad research area and attract considerable tremendous attention today in the materials science and engineering society" (Saleh et al. 2020a). Due to enhance the material properties of FGM, the static and dynamic characteristics of FG plates and beams are improved. Generally, three models can be adopted to de#ne the variation of material properties along the beam dimensions (thickness, width and length) and these models are exponential, power-law and sigmoid.

Generally, the classical beam theories are used to investigate the static and dynamic problems of beams and the main assumptions of these theories are the uniform area and homogeneous material of the beam. Several applications require enhancing the responses of the beam under various static and dynamic loads, and this enhancement in the static and dynamic responses of the beam is done by improving the material properties. For homogeneous and nonhomogeneous beams, several studies used Rayleigh Method (RM) to determine the frequency and de"ection of uniform and non-prismatic beams (Abdulsamad et al. 2021; Al-Ansari 2012;2013; Al-Ansari et al. 2018;2019; Diwan et al. 2019).

When the material properties changed in thickness-direction, several studies estimated the de"ection of uniform beam using analytical and numerical methods (Chakraborty et al. 2003; Gayen et al. 2021; Gayen 2022; Helal 2020; Li 2008; Nie et al. 2013; Şimşek et al. 2013; Zainy et al. 2018; Zhong and Yu 2007; Zhu and Sankar 2004). On the other hand, several researchers studied the e$ect of crack on static or dynamic behaviors of functionally graded beams or sha(s (Gayen et al. 2018; 2020a 2020b). For example, Gayen (2022) introduced "an exact solution for thermo-elastic behavior of radially functionally graded hollow sha(s" assuming di$erent models to describe the material properties in the radial direction such as linear law, power law and exponential law models. By using a linear strain-displacement relations and steady-state Fourier equation of heat conduction, he solved analytically thermo-elastic equations to obtain displacement and stress #elds as functions of radial distances, material gradient indices, and temperature gradients. Gayen et al. (2020a) used aluminum oxide (Al2O3) and stainless steel to represent the radially Functionally Graded sha(appling power law model. !ey studied the e$ects of temperature gradient and gradient index in addition to crack size and crack orientation on the direct and cross-couple local "exibility coe)cients in a cracked structure. Gayen et al. (2018) represented the local "exibility coe)cients as a function of crack depth using #nite element method to investigate the e$ects of crack depth, crack position, slenderness ratio, thermal gradient and gradient parameter on the free vibration of the cracked radially FG sha(. Gayen et al. (2020b) studied the e$ect of transverse surface crack in addition to temperature and material gradients on the vibration of

of radially functionally graded rotating sha(s considering nonlinear material properties applying #nite element formulation and basing on Timoshenko beam theory. !ey used power law model to describe the material properties for two types: FG sha(s (FGM I (SS/Al2O3) and FGM II (SS/ZrO2)).

Shahba et al. (2011) applied Timoshenko beam theory to investigate the vibration behavior of tapered axial-FG beam. While Nguyen, N-T et al. (2014) used Euler–Bernoulli beam theory to study the static transverse de"ection of thickness functionally graded beam (T-FGB) and axially-functionally graded beam (A-FGB) with non-uniform area, and they introduced the evaluation between the results calculated by the new model besides that of #nite element model. Nguyen et al. (2013) calculated a large de"ection of tapered cantilever axial-FG beam using the #nite elements technique and they investigated the impact of slenderness ratio and non-uniformity (type and ratio) on the transverse de"ection. Rajasekaran and Khaniki (2019) based on nonlocal strain gradient theory and used the #nite-element method for studying the mechanical behaviors of non-uniform size dependent axial-FG beam with di$erent types of materials. Lin et al. (2019) investigated the large deformation behavior of a cantilever axial-FG beam under load at a free end using the “homotopy analysis method”. !ey adopted a power-law equation to represent the mechanical and physical properties and obtained the deformation solution of axial-functionally graded beams by applying the solution of the corresponding homogeneous beam as the initial guess. !ey observed a good convergence between the analytical results and the #nite-element solutions. Soltani and Asgarian (2019) used power series technique and Timoshenko theory to develop a new solution for static and buckling behavior of axially-functionally graded beam (A-FGB). !ey studied the linear stability of nonprismatic cantilever A-FGB and they compared the new solution results with the results obtained by #nite-element method and further solutions available. Mahmoud (2019) presented a general solution of the vibration behavior of a non-uniform axial-FG beam when the A-FG beam was loaded by masses at the free end of the beam. In Daikh et al. (2022), using a “new higher order shear deformation theory”, researchers investigated the de"ection and buckling stability of axially single-walled (SW) functionally graded (FG) carbon nanotubes reinforced composite (CNTRC) plates. Walaa (2021) studied the transverse de"ection and free vibration of non-uniform axial-functionally graded beam with di$erent boundary conditions using #nite-element technique. !e material properties of the axial-functionally graded beam vary using the power-law model.

Finally, in Karamanli and !uc (2021), by applying the #nite-element method and using both a quasi-3D and modi#ed strain gradient theories, the structural problem of 2-D FG porous microbeams was investigated. !ey applied the “Hermite - cubic beam element” with various supporting types to develop and solve the di$erential equations of static de"ection, buckling, and free vibration behaviors. On the other hand, Karamanli and !uc (2018) used the #nite-element technique to calculate the deformations of

conventional functionally graded micro-beams with uniformly distributed load. !ey applied the power-law equation to represent the change of mechanical and physical properties for conventional functionally graded micro-beams.

In prior work, Wadi et al. (2022) applied the Rayleigh method to determine the static de"ection of cantilever axial-FG beam under distributed and transverse tip loads. In this work, the Rayleigh method (RM) is modi#ed to study the in"uence of di$erent material properties of the axial-FG beam along the length of a simply supported beam. !e in"uence of material distribution, modulus ratio (ME-Ratio) and load type on transverse displacement are investigated and the results estimated by Rayleigh method are evaluated to the #nite-element results, technique by employing "BEAM" element.

PROBLEM DESCRIPTION AND MATERIALS

In FGM, the material properties are changed along the length of beam using three general equations and these equations are exponential, sigmoid and power-law (Wadi et al. 2022; Walaa 2021).Now, the power-law equation (Eq. 1) is adopted to de#ne the material distribution in axial direction and the mechanical and physical properties can be described in Fig. 1:

$$P(x) = \left(P_L - P_R\right) * \left(1 - \left(\frac{x}{L}\right)\right)^n + P_R \qquad (1)$$

Where: PL and PR are the properties at the le(and right beam end, respectively; P(x) is the property at any point along the length of the beam; (x) is the position of the point starting from the le(side of the beam; (L) is the length of the axial-functionally graded beam, and (n) is the power-law index. Generally, the de"ection of any axial-FGB a$ects the "sti$ness" of this beam, and the "sti$ness" of FGB is the multiplication of "modulus of the elasticity (E) and second moment of area (I)". In axial-FGB, the beam modulus changes in axial-direction, therefore, the sti$ness of FGB changes too. !e de"ection of an axial-functionally graded beam is a$ected by the supporting conditions, type of applied load, modulus ratio of the parents and power-law index.

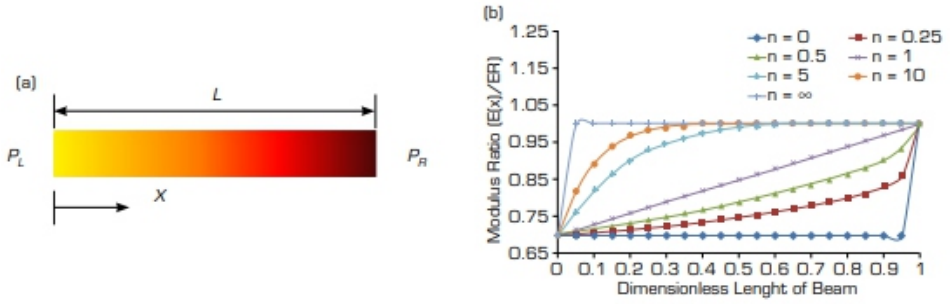

Source: Elaborated by the authors.

Figure 1. Variation of Material Properties in Axial Direction.

RAYLEIGH METHOD

!e non-uniformity area and non-homogenous mechanical and physical properties cause a variation in sti$ness of beam, and the calculation of “equivalent sti$ness” of uniform simply supported axial-functionally graded beam is the main challenge in Rayleigh method (RM). Firstly, the equivalent sti$ness of the axial-FGB is estimated and then the de"ection at any point in the axial-functionally graded beam is determined. !e following points are used to determine the de"ection:

• !e axial-FGB is divided into (M) segments and the number of points is (M+1).

• !e elastic modulus and Poisson’s ratio at each point (m point) using Eqs. 2 and 3 when the location of any point in direction is determined by (x = ǻx*i) where (ǻx=L/M) and i=1,2,3,….M+1 (see Fig. 2).

$$E(x) = \left(E_L - E_R\right) * \left(1 - \left(\frac{x}{L}\right)\right)^n + E_R$$
$$E(i) = \left(E_L - E_R\right) * \left(1 - \left(\frac{\Delta x * i}{L}\right)\right)^n + E_R ; i = 1, 2, 3, \ldots\ldots M + 1 \quad (2)$$

$$\nu(x) = \left(\nu_L - \nu_R\right) * \left(1 - \left(\frac{x}{L}\right)\right)^n + \nu_R$$
$$\nu(i) = \left(\nu_L - \nu_R\right) * \left(1 - \left(\frac{\Delta x * i}{L}\right)\right)^n + \nu_R ; i = 1, 2, 3, \ldots\ldots M + 1 \quad (3)$$

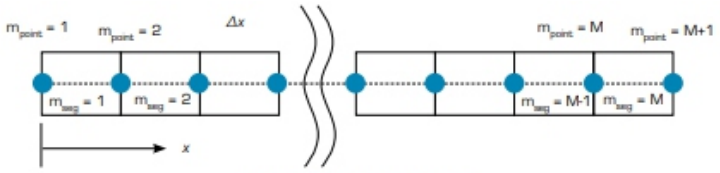

Source: Elaborated by the authors.

Figure 2. The Division and Numbering of A-FG Beam.

• In each segment, the elastic modulus and Poisson’s ratio are estimated in Eq. 4 and 5:

$$E\left(x + \left(\frac{\Delta x}{2}\right)\right) = \frac{(E(x)+E(x+\Delta x))}{2}$$
$$E(j) = \frac{(E(i)+E(i+1))}{2} ; j = 1, 2, 3, \ldots\ldots M \quad (4)$$
$$\nu\left(x + \left(\frac{\Delta x}{2}\right)\right) = \frac{(\nu(x)+\nu(x+\Delta x))}{2}$$

$$\nu(j) = \frac{(\nu(i)+\nu(i+1))}{2} ; j = 1, 2, 3, \ldots\ldots M \quad (5)$$

The equivalent sti$ness of the simply supported axial-functionally graded beam is determined by:

• !e center of the area of the axial-functionally graded beam (Xc

$$X_c = \frac{\sum_{j=1}^{M} X_j * A_j}{\sum_{j=1}^{M} A_j} \quad (6)$$

Where Aj is the cross section area of (j) segment. !e center of axial-functionally graded beam in this work is (0.5*L), because it has a uniform area.

• !e simply supported axial-functionally graded beam is divided into two cantilever beams as shown in Fig. 3.

• !e "equivalent sti$ness" of free-clamped and clamped-free axial-FG beams are estimated depending on the supporting type (Clamped – Free or Free - Clamped A-FG beam) using Eq 7 and 8 (for more details, see Abdulsamad et al. (2021), Al-Ansari (2012; 2013), Al-Ansari et al. (2018; 2019), Diwan et al. (2019), Wadi et al. (2022), Zainy et al. (2018)):

$$\left((EI)_{eq}\right)_L = \frac{(L_{Left})^3}{\sum_{k=1}^{M_{Left}} \frac{(L_k)^3-(L_{k-1})^3}{(EI)_k}} ; K = 1, 2, ... M_{Left} \quad (7)$$

$$\left((EI)_{eq}\right)_R = \frac{(L_{Right})^3}{\sum_{k=1}^{M_{Right}} \frac{(L_k)^3-(L_{k-1})^3}{(EI)_k}} ; K = 1, 2, ... M_{Right} \quad (8)$$

The total equivalent stiffness is (Eq. 9):

$$(EI)_{eq} = \frac{\left(L_{Right}+L_{Left}\right)*\left(L_{Right}\right)^2*\left(L_{Left}\right)^2}{\left(\left(\sum_{K=1}^{M_{Right}} \frac{I_{K-1}^3-I_K^3}{I_K}\right)*L_{Right}^2\right)+\left(\left(\sum_{K=1}^{M_{Left}} \frac{I_K^3-I_{K-1}^3}{I_K}\right)*L_{Left}^2\right)} \quad (9)$$

Where: $L_{Left} + L_{Right} = L$ and in this work $L_{Left} + L_{Right} = L/2$

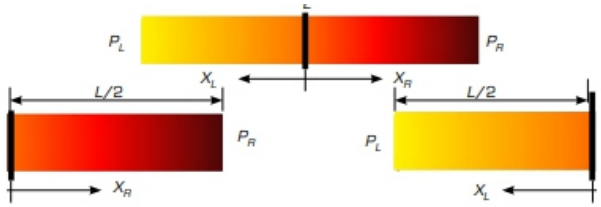

Source: Elaborated by the authors.

Figure 3. Dividing the Simply Supported A-FG Beam From the Center of Area into Two Cantilever A-FG Beams.

• The defections of simply supported axial-functionally graded beam are estimated using the Eq. 10:

$$[Y] = [\delta][F] \quad (10)$$

Where: [Y] is the de"ection matrix, [δ] is delta matrix using Fig. 4 to estimate this matrix assuming W=1, and [Y] = f I where i = 1, 2, 3, ... M + 1 is the force matrix and when the distributed load (ω) (N/m) is applied, the values of fI are calculated in Eq. 11:

$$f_i = \{\frac{\omega^*\Delta x}{2} \; when \; i = 1 \; and \; i = M + 1 \quad \omega * \Delta x \; when \; i \neq 1 \; and \; i \neq M + 1$$

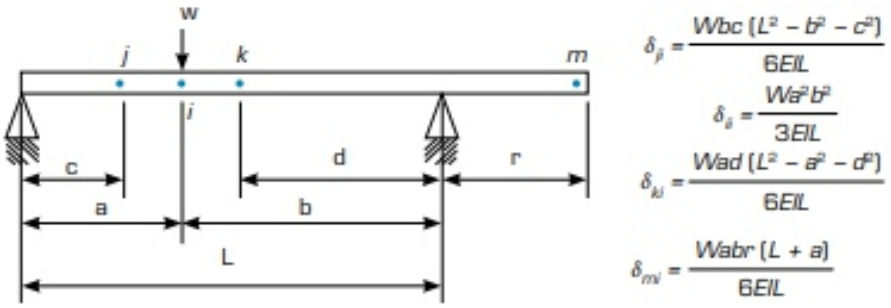

Source: Retrieved from Walaa (2021).

Figure 4. De"ections Formula of Simply Supported Beam at Di$erent Points.

The calculating procedure, described in this section, is programmed using FORTRAN Power Station.

FINITE ELEMENT MODEL

In this work, the commercial so(ware ANSYS APDL is used to simulate the simply supported A-FG beam to study the static de"ection under the uniform-distributed load. !e “BEAM189” is used and the properties and characteristics of this element is “!e BEAM189 element is suitable for analyzing slender to moderately stubby/thick beam structures. !e element is based on Timoshenko beam theory which includes shear-deformation e$ects. !e element provides options for unrestrained warping and restrained warping of cross-sections. !e element is a quadratic three-node beam element in 3-D. With default settings, six degrees of freedom occur at each node; these include translations in the x, y, and z directions and rotations about the x, y, and z directions. An optional seventh degree of freedom (warping magnitude) is available. !e element is well-suited for linear, large rotation, and/or large-strain nonlinear applications” (ANSYS, Inc., 2016, ANSYS Version 17.2).

In ANSYS model, the axial-functionally graded beam is divided into 20 parts and the part is also divided into 5 elements to apply the convergence criteria discussed by Wadi et al. (2022). !e A-FG beam in ANSYS so(ware is drawn using twenty-one key points and the twenty lines which represent twenty segments. !e elastic modulus and Poisson ratio of each segment are calculated using Eq. 4 and 5 (i.e. M=20 in ANSYS model).

Accuracy of the Present Models:

In order to exam the accuracy of Rayleigh and FE models, was there a comparison between the non-dimensional de"ection estimated by Rayleigh and FE models and that obtained by Walaa (2021). Walaa (2021) applied 2-D FE model using ANSYS Workbench.

In this study, dimensions of axial-FGB and mechanical properties are listed in Table 1 and 2 respectively. !e non-dimensional static de"ection can be determined by the Eq. 12:

$$Y(x) = \frac{y(x)}{\left(y_{max.}\right)_{at\ n=0}} \qquad (12)$$

Where: Y(x) is the non-dimensional static de"ection at any point (x) in axial-direction. y(x) is the static de"ection at any point (x) in axial-direction. (ymax.)at n = 0 is the maximum static de"ection at zero power index (n=0).

Table 1. The Used Dimensions of the Axial-FGB.

No.	Dimension	Magnitude
1	Length of Beam (l)	1 meter
2	Width of Beam (W)	0.01 meter
3	Thickness of Beam (h)	0.01 meter

Source: Elaborated by the authors.

Table 2. The Mechanical Properties of Le(and Right Materials of the Axial-FGB.

Material	Property	Magnitude
Metal (Right Material)	Elastic Modulus of (E_R)	210 G Pa.
	Poisson Ratio (ν_R)	0.3
	Density (ρ_R)	7800 kg/m³
Ceramic (Left Material)	Elastic Modulus (E_L)	390 G Pa.
	Poisson Ratio (ν_L)	0.23
	Density (ρ_L)	3960 kg/m³

Source: Retrieved from Walaa (2021).

Figure 5 illustrates the comparison between the maximum non-dimensional static de"ection estimated by present models and obtained by Walaa (2021), while Fig. 6 shows the discrepancy percentage of the Rayleigh and 1D ANSYS results with respect to Walaa results. From Fig. 5 and 6, an excellent agreement is found between the results of Rayleigh method and that calculated by ANSYS so(ware: the maximum discrepancy percentage is smaller than 2.5 % when the power-law index is approximately 1.5 and then the discrepancy percentage decreases with increasing power-law index (i.e. when the power-law index increase, the A-FG beam tend to be pure ceramic).

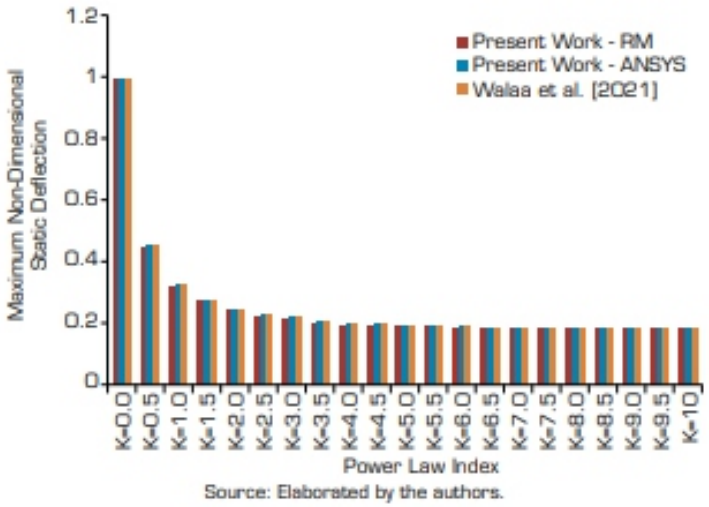

Source: Elaborated by the authors.

Figure 5. The Comparison Between the Non-Dimensional Static Deflection of the Present Model and That Calculated by Walaa (2021).

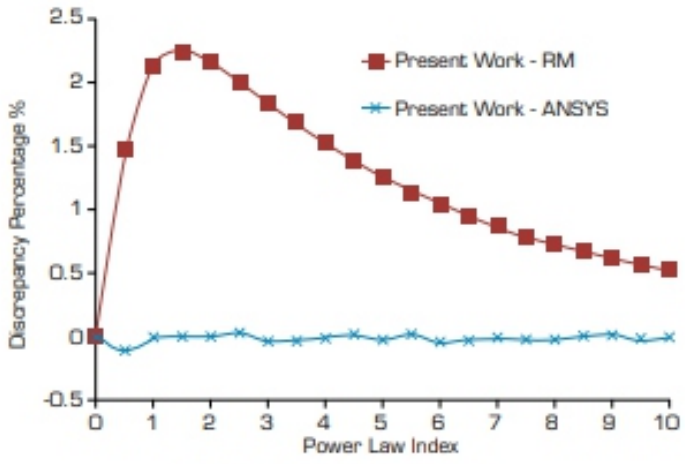

Source: Elaborated by the authors.

Figure 6. The Discrepancy Percentage of the Present Model with Respect to Results of Walaa (2021).

RESULTS AND DISCUSSION

In addition to the accurateness of the present numerical models, the in"uences of two important parameters (modulus-ratio (ME-Ratio) and power-law index (material distribution index)) on the non-dimensional static de"ection of a simply supported A-FG beam are studied in this work. !e power-law index (n) refers to the material distribution along the A-FG beam and it changes from (0 to 100).

Modulus ratio (ME-Ratio) refers to the ratio of the elastic moduli of the parents of A-FG beam (i.e. EL/ER),in other words, it also refers to materials positions at the two ends of the A-FG beam. !e values of modulus ratio (ME-Ratio), used in this work, are (0.25, 0.5, 0.75, 1, 1.333, 2 and 4).

Figure 7 illustrates the e$ect of power-law index (n) on the maximum non-dimensional static de"ection of a simply supported A-FG beam at a di$erent elastic moduli ratio (ME-Ratio). Generally, the maximum non-dimensional static de"ection changes sharply when the power-law index is smaller than (10). !is change in maximum non-dimensional static de"ection is a$ected by the value of elastic moduli ratio (ME-Ratio). When the elastic moduli ratio (ME-Ratio) equals 1, the A-FG beam has a homogenous properties (i.e. pure material), in this case, the maximum non-dimensional static de"ection is constant because the e$ective modulus of FG beam is constant. If the elastic moduli ratio (ME-Ratio) is smaller than 1 (i.e. ER>EL) , the maximum non-dimensional static de"ection increases with increase of the power law index (n), because the e$ective modulus of FG beam decreases with the increasing of the power law index (n) and equal to ER at n>10 (i.e. the e$ective modulus →ER). But, the maximum non-dimensional static de"ection decreases with the increase of the power law index (n) when the elastic moduli ratio (ME-Ratio) is more than 1 (i.e. ER<EL).

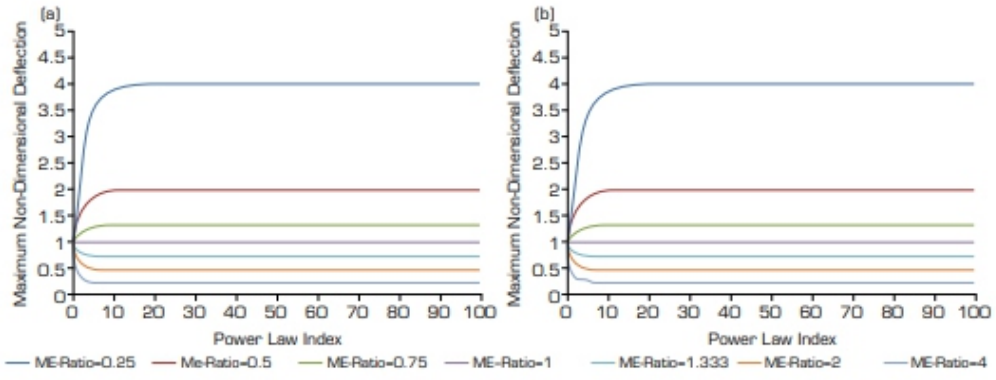

Source: Elaborated by the authors.

Figure 7. The Variation of the Maximum Non-Dimensional Static De"ection Due to an Increase in the Material Distribution Index (n) at Di$erent Elastic Moduli Ratio (ME-Ratio) for the Present Models (a) Rayleigh Method (RM); (b) ANSYS- 1D Model.

When power-law index equals zero (i.e. the material of axial-FGB is pure right material) (see Eq. 1), the maximum non dimensional static de"ection is not a$ected by the elastic modulus ratio (ME-Ratio) because the increase of elastic modulus ratio (ME-Ratio) is made by increasing the modulus of le(material (EL). !e maximum non-dimensional static de"ection with the increase of the elastic moduli ratio (ME-Ratio) for any power-law index (n,) and the rate of decreasing of maximum non-dimensional static de"ection reduces with increasing power-law index (n) as displayed in Fig. 8

For more comparison between the present models (ANSYS- 1D Model and Rayleigh Method (RM)), Fig. 9 illustrates the convergence between the results of non- dimensional static de"ection calculated be the two models.

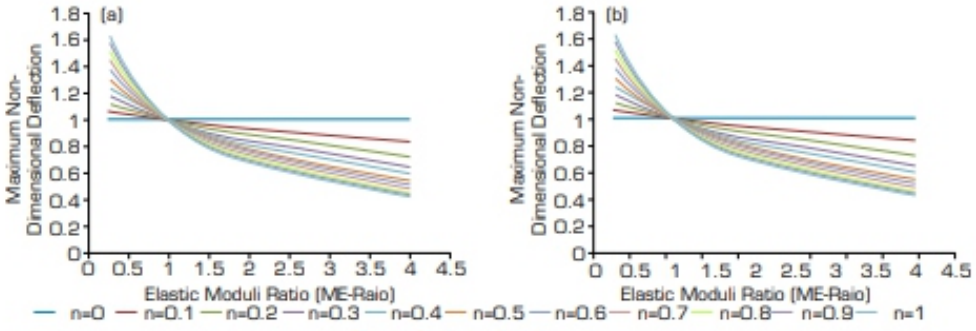

Source: Elaborated by the authors.

Figure 8. The Variation of the Maximum Non-Dimensional Static Deflection Due to increase Elastic Moduli Ratio (ME-Ratio) at Different Material Distribution Index (n) for the Present Models (a) Rayleigh Method (RM); (b) ANSYS- 1D Model.

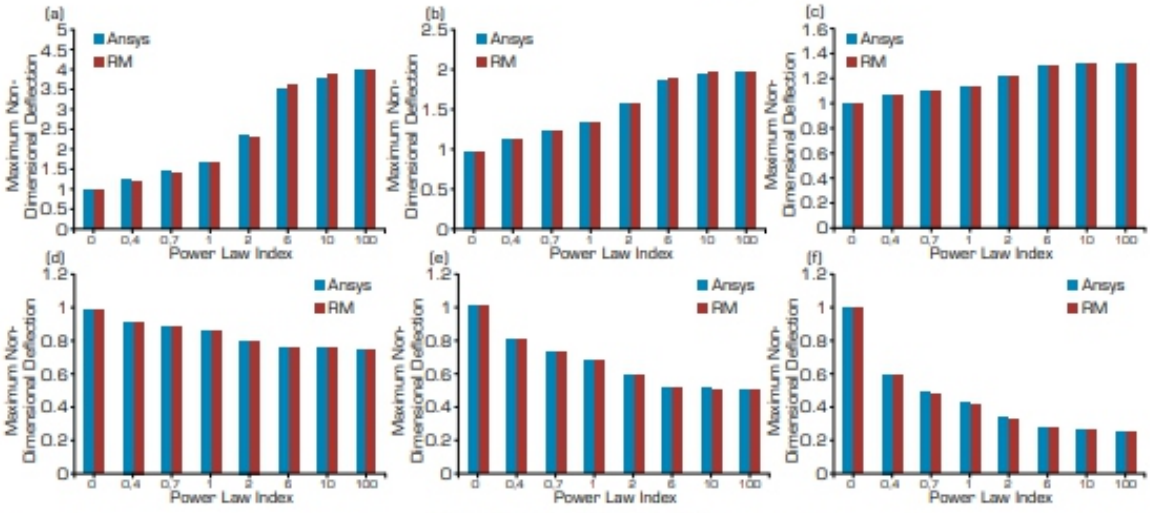

Source: Elaborated by the authors.

Figure 9. Comparison Between Non-Dimensional Static Deflections Calculated by ANSYS-1D Model and Rayleigh Method (RM) for Different Power-law Index (n) and Elastic Moduli Ratio (ME-Ratio). (a) ME-Ratio = 0.25; (b) ME-Ratio = 0.5; (c) ME-Ratio = 0.75; (d) ME-Ratio = 1.333; (e) ME-Ratio = 2; (f) ME-Ratio = 4.

Figure 10 shows the pro#le of non-dimensional static de"ection at any point on the axial direction for di$erent elastic moduli ratio (ME-Ratio) and power-law index (n). Similar notes can be seen for the non-dimensional static de"ection at any point in the axial-direction of axial-FGB comparing with the curves of maximum non-dimensional static de"ection (i.e. Fig. 7 and 8). When the elastic moduli ratio (ME-Ratio) equals 1 or the power-law index (n) equals zero, the axial-FGB has homogenous properties (i.e. pure material) and the non dimensional static de"ection is constant. If (ER>EL), the non-dimensional static de"ection increases due to an increase of the power-law index (n) while the non-dimensional static de"ection decreases with an increase of the power-law index (n), if (ER<EL). !e non-dimensional static de"ection increases with the decrease of the elastic moduli ratio (ME-Ratio) for any power-law index (n) and the rate of decreasing of non-dimensional static de"ection reduces with increasing power-law index

(n) and the rate of decreasing of non-dimensional static de"ection reduces with increasing power-law index (n). But the position of the maximum non-dimensional static de"ection calculated by ANSYS 1D model does not appear at the mid span of A-FG beam and there is a small deviation in position of maximum non-dimensional static de"ection. !isdeviation in position of maximum non-dimensional static de"ection is shown in Fig. 11 and it decreases when the power-law index increases. Also, the deviation ME-Ratio =0.25 is similar to the deviation when ME-Ratio =4. !is symmetrical deviation pro#le is also found for each value of elastic moduli ratio and its inverse (i.e. ME-Ratio and (1/ ME-Ratio)). !ere is no deviation in position of maximum non-dimensional static de"ection when ME-Ratio =1, because the beam is homogenous and uniform at the same time. !e value of the deviation increases when the elastic moduli ratio (ME-Ratio) diverges from 1. Finally, the deviation in position of maximum non-dimensional static de"ection is not found in the results of Rayleigh Method.

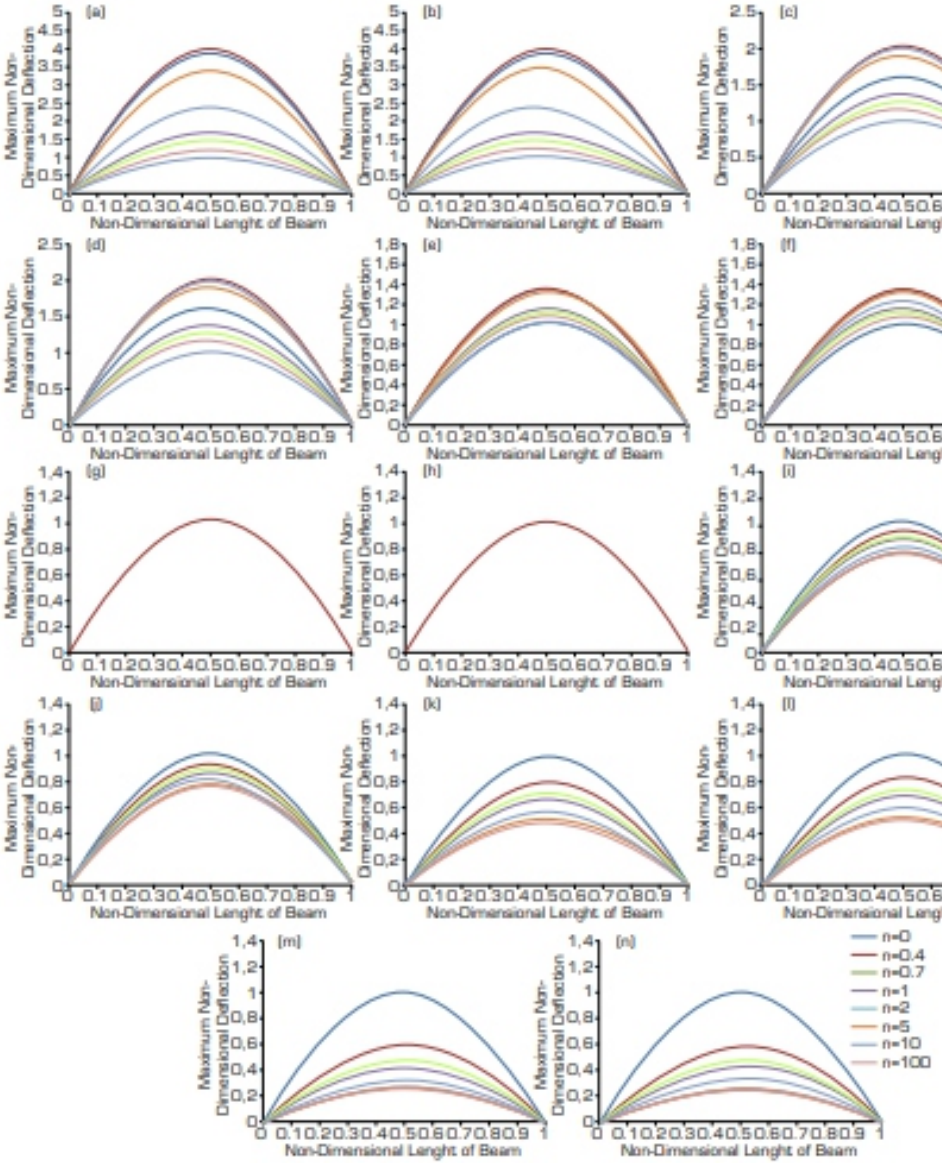

Figure 10. Comparison Between Non-Dimensional Static De"ections Along the Dimension Length of FG Beam Calculated by ANSYS- 1D Model and Rayleigh Method (RM) for Di$erent Power-law Index (n) and Elastic Moduli Ratio(ME-Ratio). (a) Rayleigh Method (RM), ME-Ratio = 0.25; (b) ANSYS- 1D Model, ME-Ratio = 0.25; (c) Rayleigh Method (RM),ME-Ratio = 0.5; (d) ANSYS- 1D Model, ME-Ratio = 0.5; (e) Rayleigh Method (RM), ME-Ratio = 0.75; (f) ANSYS- 1D Model,ME-Ratio = 0.75; (g) Rayleigh Method (RM), ME-Ratio = 1; (h) ANSYS- 1D Model, ME-Ratio = 1; (i) Rayleigh Method (RM),ME-Ratio = 1.333; (j) ANSYS- 1D Model, ME-Ratio = 1.333; (k) Rayleigh Method (RM), ME-Ratio = 2; (l) ANSYS- 1D Model,ME-Ratio = 2; (m) Rayleigh Method (RM), ME-Ratio = 4; (n) ANSYS- 1D Model, ME-Ratio = 4.

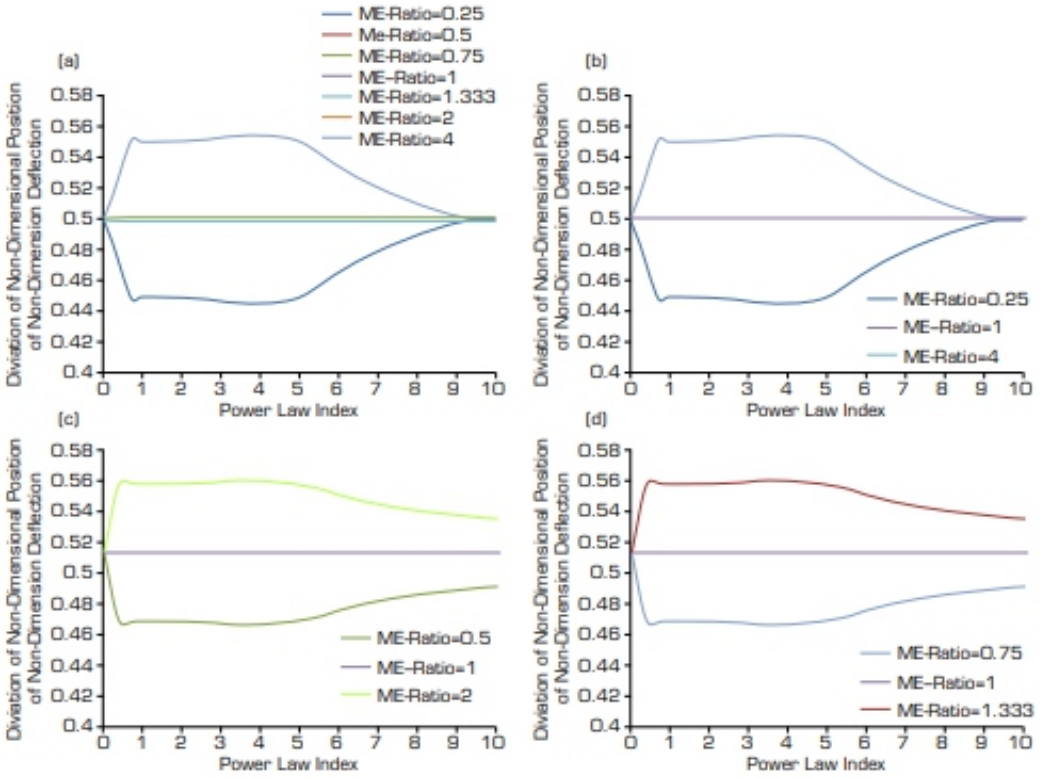

Source: Elaborated by the authors.

Figure 11. Deviation of Non-Dimensional Position of Maximum Non-Dimensional Static De"ection Calculated by ANSYS-1 D Model at Di$erent Power-law Index (n) and Elastic Moduli Ratio (ME-Ratio). (a) Total ME-Ratio; (b) ME-Ratio=0.25,1 and 4; © ME-Ratio=0.5,1 and 2; (d) ME-Ratio=0.75,1 and 1.333.

CONCLUSIONS

In this work, two numerical models are built for the studying of the de"ection of a simply supported axial-functionally graded beam, the Rayleigh method is adopted to build the #rst model (new one) while the second model used the #nite element technique to build 1 D – model utilizing the ANSYS APDL. In addition to the accuracy of the two models, the e$ects of elastic moduli ratio (ME-Ratio) and material distribution (n) on the maximum static de"ection and its position are studied. From the #gures, these points are concluded:

•The new model based on Rayleigh method gives results with an excellent agreement with the results of ANSYS– 1D model and available literatures;

•The A-FG beam has homogenous properties when the elastic moduli ratio (ME-Ratio) equals 1 or the power-law index (n) equal zero and in this case, the non-dimensional static de"ection and its maximum are constant;

•The non-dimensional static de"ection and its maximum decrease with the increase of the power-law index (n) when (ER<EL). If (ER>EL), the non-dimensional static de"ection and its maximum increase with the increase of the power-law index

• The non-dimensional static deflection increases with the decrease of the elastic moduli ratio (ME-Ratio) for any power-law index (n) and the rate of the decreasing of non-dimensional static deflection reduces with power-law index (n);

• In ANSYS– 1D model only, the position of the maximum non-dimensional static de"ection is deviated from the mid span of A-FG beam and this deviation in position of maximum non-dimensional static de"ection decreases when the power-law index increases and increases when the elastic moduli ratio (ME-Ratio) diverges from 1.

• The deviation in position of maximum non-dimensional static de"ection is not found in the results of the Rayleigh method.

In future work, the de"ection and dynamic behavior of non-prismatic simply supported axial-functionally graded beams will be investigated considering the e$ect of symmetrical and unsymmetrical boundary conditions.

CONFLICT OF INTEREST

Nothing to declare.

DATA AVAILABILITY STATEMENT

All dataset were generated or analyzed in the current study.

AUTHOR CONTRIBUTIONS

Conceptualization: Shukur ZM; Formal analysis: Hamad RF, Ali YK; Research: Hamad RF, Al-Karaishi M; Methodology:

Al-Ansari LS, Shukur ZM; So!ware: Al -Ansari LS; Supervision: Al-Ansari LS, Shukur ZM; Validation: Al-Ansari LS, Shukur ZM; Writing - Preparation of original dra!: Al-Ansari LS, Shukur ZM; Writing - Proofreading and editing: Al-Ansari LS, Shukur ZM.

FUNDING

Not applicable.

ACKNOWLEDGMENTS

Not applicable.

REFERENCES

Abdulsamad HJ, Wadi KJ, Al-Raheem SK, Al-Ansari LS (2021) Investigation of Static De"ection in Internal Stepped Cantilever Beam. Journal of Mechanical Engineering Research and Developments 44(5):87-125.

Al-Ansari LS (2012) Calculating of Natural Frequency of Stepping Cantilever Beam. Int J Mech Mechatron Eng 12(5):59-68.

Al-Ansari LS (2013) Calculating Static De"ection and Natural Frequency of Stepped Cantilever Beam Using Modi#ed Rayleigh Method. IJMPERD 3(4):107-118.

Al-Ansari LS, Al-Hajjar AMH, Jawad H (2018) Calculating the natural frequency of cantilever tapered beam using classical Rayleigh, modi#ed Rayleigh and #nite element methods. Int J Eng Technol 7(4):4866-4872.

Al-Ansari LS, Zainy HZ, Yaseen AA, Aljanabi M (2019) Calculating the natural frequency of hollow stepped cantilever beam. Int J Mech Eng Technol 10(1):898-914.

Ashby MF (2000) Materials Selection in Mechanical Design. Oxford: Butterworth-Heinemann.

Bhavar V, Kattire P, !akare S, Patil S, Singh RKP (2017) A Review on Functionally Gradient Materials (FGMs) and !eir Applications. IOP Conf Ser: Mater Sci Eng 229(1):012021.

Diwan AA, Al-Ansari LS, Al-Sa$ar AA, Al-Anssari QS (2022) Experimental and theoretical investigation of static de"ection and natural frequency of stepped cantilever beam. Aust J Mech Eng 20(2):303-315. https://doi.org/10.1080/14484846.2019.1704494.

Ebhota WS, Jen T-C (2018) Casting and Applications of Functionally Graded Metal Matrix Composites. In: Vijayaram TR, editors. Advanced Casting Technologies. InTech. https://doi.org/10.5772/intechopen.71225.

El-Galy IM, Bassiouny BI, Ahmed MH (2018) Empirical model for dry sliding wear behaviour of centrifugally cast functionally graded Al/SiCp composite. Key Eng Mater 786:276-285. https://doi.org/10.4028/www.scienti#c.net/KEM.786.276.

Gayen D, Chakraborty D, Tiwari R (2018) Free Vibration Analysis of Functionally Graded Sha(System with a Surface Crack. J Vib Eng Technol 6:483-494. https://doi.org/10.1007/s42417-018-0065-9

Gayen D, Chakraborty D, Tiwari R (2020a) Determination of Local Flexibility Coe)cients of a Functionally Graded Sha(with Breathing Crack. In: Dutta S, Inan E, Dwivedy S editors. Advances in Rotor Dynamics, Control, and Structural Health Monitoring. Lecture Notes in Mechanical Engineering. Singapore: Springer. https://doi.org/10.1007/978-981-15-5693-7_13

Gayen D, Chakraborty D, Tiwari R (2020b) Transverse Vibration and Stability of a Cracked Functionally Graded Rotating Sha(System. In: Li L, Pratihar D, Chakrabarty S, Mishra P, editors. Advances in Materials and Manufacturing Engineering.

Lecture Notes in Mechanical Engineering. Singapore: Springer. https://doi.org/10.1007/978-981-15-1307-7_71.

Gayen D, Tiwari R, Chakraborty D (2021) !ermo-Mechanical Analysis of a Rotor-Bearing System Having a Functionally

Graded Sha(with Transverse Breathing Cracks. In: Rao JS, Arun Kumar V, Jana S editors. Proceedings of the 6th National Symposium on Rotor Dynamics. Lecture Notes in Mechanical Engineering. Singapore: Springer. https://doi.org/10.1007/978- 981-15-5701-9_8

Gayen D (2022) Analysis of Temperature, Displacement, and Stress in Sha(s Made of Functionally Graded Materials with

Various Grading Laws. Adv Eng Mater 24(5):2101328. https://doi.org/10.1002/adem.202101328

Harris B (1999) Engineering Composite Materials. London: Institute of Materials.

Helal SHB (2020) !e Static Analysis of a Functionally Graded Euler Beam under Mechanical Loads (Master !esis). Kufa: University of Kufa.

Jamian S (2012) Application of functionally graded materials for severe Plastic Deformation and Smart Materials: Experimental Study and Finite Element Analysis (Doctoral dissertation). Nagoya: Nagoya Institute of Technology.

Kalyan V, Swamy SB, Snehith N, Karthik UPS, Ommi NS (2017) A review on application of polymers in mechanical engineering. Int J Adv Res Sci Eng 6(11):1972-1979.

Karamanli A, !uc PV (2018) Size dependent bending analysis of two directional functionally graded microbeams via a quasi-3D theory and #nite element method. Compos B Eng 144:171-183. https://doi.org/10.1016/j.compositesb.2018.02.03

Karamanli A, !uc PV (2021) Bending, vibration, buckling analysis of bidirectional FG porous microbeams with a variable material length scale parameter. Appl Math Model 91:723-748. https://doi.org/10.1016/j.apm.2020.09.058

Kassner ME, Smith KK, Campbell CS (2015) Low-temperature creep in pure metals and alloys. J Mater Sci 50:6539-6551. https://doi.org/10.1007/s10853-015-9219-2.

Kaw AK (2006) Mechanics of Composite Material. Boca Raton: Taylor & Francis Group.

Li X-F (2008) A uni#ed approach for analyzing static and dynamic behaviors of functionally graded Timoshenko and Euler–

Bernoulli beams. J Sound Vibr 318(4-5):1210-1229. https://doi.org/10.1016/j.jsv.2008.04.056

Lin X, Huang Y, Zhao Y, Wang T (2019) Large deformation analysis of a cantilever beam made of axially functionally graded material by homotopy analysis method. Appl Math Mech 40:1375-1386. https://doi.org/10.1007/s10483-019-2515-9

Mahmoud MA (2019) Natural frequency of axially functionally graded, tapered cantilever beams with tip masses. Eng Struct 187:34-42. https://doi.org/10.1016/j.engstruct.2019.02.043

Majeed T, Wahid MA, Sharma N (2017) Ceramic materials: processing, joining and applications. Paper presented at International Conference On Communication & Computational Technologies by RIET, Jaipur & IJCRT.ORG. Jaipur, India.

Nguyen DK (2013) Large displacement response of tapered cantilever beams made of axially functionally graded material.

Composites: Part B 55:298-305. https://doi.org/10.1016/j.compositesb.2013.06.024

Nguyen N-T, Kim N-I, Cho I, Phung QT, Lee J (2014) Static analysis of transversely or axially functionally graded tapered beams. Materials Research Innovations 18(Suppl 2):260-264. https://doi.org/10.1179/1432891714Z.000000000419

Nie GJ, Zhong Z, Chen S (2013) Analytical solution for a functionally graded beam with arbitrary graded material properties.

Compos Pt B-Eng 44(1):274-282. https://doi.org/10.1016/j.compositesb.2012.05.029.

Osswald TA (2010) Material Science of Polymers for Engineers. Ohio: Hanser Publications.

Rajasekaran S, Khaniki HB (2019) Finite element static and dynamic analysis of axially functionally graded nonuniform small-scale beams based on nonlocal strain gradient theory. Mech Adv Mater Struct 26(14):1245-1259. https://doi.org/10.1 080/15376494.2018.1432797

Saleh B, Jiang J, Ma A, Song D, Yang D (2019) E$ect of main parameters on the mechanical and wear behaviour of functionally graded materials by centrifugal casting: a review. Met Mater Int 25:1395-1409. https://doi.org/10.1007/s12540-019-00273-8

Saleh B, Fathi JJR, Al-hababi T, Xu Q, Wang L, Song D, Ma A (2020a) 30 Years of functionally graded materials: An overview of manufacturing methods, Applications and Future Challenges. Composites Part B 201:108376. https://doi.org/10.1016/j.compositesb.2020.108376.

Saleh B, Jiang J, Fathi R, Xu Q, Wang L, Ma A (2020b) Study of the microstructure and mechanical characteristics of Az91–SiCp composites fabricated by stir casting. Arch Civ Mech Eng 20:71. https://doi.org/10.1007/s43452-020-00071-9

Saleh B, Jiang J, Xu Q, Fathi R, Ma A, Li Y, Wang L (2021) Statistical analysis of dry sliding wear

Saleh B, Jiang J, Fathi R, Xu Q, Wang L, Ma A (2020b) Study of the microstructure and mechanical characteristics of Az91–SiCp composites fabricated by stir casting. Arch Civ Mech Eng 20:71. https://doi.org/10.1007/s43452-020-00071-9.

Saleh B, Jiang J, Xu Q, Fathi R, Ma A, Li Y, Wang L (2021) Statistical analysis of dry sliding wear process parameters for Az91 alloy processed by RD-ECAP using response surface methodology. Met Mater Int 27:2879-2897. https://doi.org/10.1007/s12540-020-00624-w.

Shahba A, Attarnejad R, Marvi MT, Hajilar S (2011) Free vibration and stability analysis of axially functionally graded tapered Timoshenko beams with classical and non-classical boundary conditions. Compos Part B 42(4):801-808. https://doi.org/10.1016/j.compositesb.2011.01.01.

Shao W (2018) Research and Application of Engineering Ceramic Material Processing Technology. IOP Conf Ser: Mater Sci Eng 394(3):032030 https://doi.org/10.1088/1757-899X/394/3/032030

Şimşek M, Kocatürk T, Akbaş ŞD (2013) Static bending of a functionally graded microscale Timoshenko beam based on the modi#ed coupling stress theory. Compos Struct 95:740-747. https://doi.org/10.1016/j.compstruct.2012.08.036.

Soltani M, Asgarian B (2019) Finite element formulation for linear stability analysis of axially functionally graded nonprismatic Timoshenko beam. Int J Struct Stabil Dynam 19(2):1950002. https://doi.org/10.1142/S0219455419500020.

Wadi KJ, Yadeem JM, Khazaal SM, Al-Ansari LS Abdulsamad HJ (2022) Static de"ection calculation for axially FG cantilever beam under uniformly distributed and transverse tip loads. Res Eng 14:100395. https://doi.org/10.1016/j.rineng.2022.100395.

Walaa MH (2021) Static and Dynamic Analysis of Axially FG Beam (doctoral dissertation). Kufa: University of Kufa.

Xu Q, Ma A, Li Y, Saleh B, Yuan Y, Jiang J, Ni, C (2019) Enhancement of mechanical properties and rolling formability in AZ91 alloy by RD-ECAP processing. Materials 12(21):3503. https://doi.org/10.3390/ma12213503.

Xu Q, Ma A, Saleh B, Li Y, Yuan Y, Jiang J, Ni C (2020) Enhancement of strength and ductility of SiCp/AZ91 composites by RD-ECAP processing. Mater Sci Eng A 771:138579. https://doi.org/10.1016/j.msea.2019.138579

Zainy HZ, Al-Ansari LS, Al-Hajjar AM, Mahdi M, Shareef S (2018) Analytical and numerical approaches for calculating the static de"ection of functionally graded beam under mechanical load. Int J Eng Technol 7(4):3889-3896.

Zhong Z, Yu T (2007) Analytical solution of a cantilever functionally graded beam. Compos Sci Technol 67(3-4):481-488. https://doi.org/10.1016/j.compscitech.2006.08.023

Zhu H, Sankar BV (2004) A combined Fourier series–Galerkin method for the analysis of functionally graded beams. J Appl Mech 71(3):421-424. https://doi.org/10.1115/1.175118.

Experimental Investigation of the Electrical Wiring Con!guration of the HK40 Hall

Ugur Kokal1 , Nazli Turan1 , Murat Celik1
Bog˘aziçi University – Department of Mechanical Engineering – Istanbul – Turkiye.

ABSTRACT

Vacuum chambers providing a low pressure environment similar to the vacuum environment in low earth orbit have been used for the testing of plasma thrusters. A signi!cant proportion of research on the e"ects of vacuum facility on plasma thrusters has focused on the e"ects of background pressure and plume expansion; however, the electrical interaction of the conductive chamber walls with the plasma thrusters needs to be explored further. In this study, the operation of a prototype Hall thruster, HK40, was investigated to understand the e"ects of wiring con!guration of the thruster-cathode-chamber system. During the tests, the thruster was operated in two di"erent grounding con!gurations. A resistance analogy regarding the changes in electrical potentials and measured currents was introduced. #e calculated thrust and e$ciency values of the two con!gurations were compared. #is study shows that the current extracted from the emitter surface of the cathode, along with the cathode-to-ground voltage can be used to estimate the thrust and thruster e$ciency. In addition, the theoretical predictions were compared with the values based on the measurements made with an in-house-built inverted pendulum type thrust stand. #e presented results show that the thrust and e$ciency values are predicted with 3.4% and 8.3% uncertainty, respectively.

Keywords: Electric propulsion; Hall thrusters; Vacuum chambers; Hollow cathodes.

I. INTRODUCTION

Space propulsion systems are used for propulsive needs of satellites in orbit or spacecra% for deep space missions (MartinezSanchez and Pollard 1998; Mazou"re 2016). While the chemical propulsion systems currently present the only viable solution for launch vehicles and are unquestionably more suitable for maneuvers that require fast burns due to their much higher thrust levels, electric propulsion systems can provide the same delta-V while consuming much less propellant compared to their counterparts. Among electric propulsion concepts, Hall thrusters are the most employed type for commercial operations and earth-orbiting satellites (Frieman et al. 2016; Lev et al. 2019; Potrivitu et al. 2020; Huo 2022). As Hall thrusters gain &ight heritage, they are also being increasingly considered for deep space missions (Brophy et al. 2012; Levchenko et al. 2018).

#e characterization and lifetime testing of the electric propulsion systems are conducted inside vacuum chamber test facilities. #ese vacuum test facilities provide the vacuum environment similar to low earth

orbit with the background pressure levels on the order of 10−5 Torr. Although, there are a vast number of studies concerning the e"ects of background pressure on thruster operation and plume expansion (Diamant et al. 2014; Huang et al. 2014; Brown and Gallimore 2011; Nakles and Hargus Junior 2011; MacDonaldTenenbaum et al. 2019; Ortega et al. 2020; Cichocki et al. 2020; Walker 2005), the possible electrical current interactions with the chamber walls and the e"ect of electrical wiring con!guration need to be investigated further (Frieman et al. 2016, Walker et al. 2016a; Frieman et al. 2014). In laboratory experiments, the walls of the vacuum chamber are electrically grounded; however, this condition is not an accurate representation of the actual &ight environment where no such electrical ground would be present. Furthermore, magnetic !eld topology and cathode position yield multifaceted interactions with the chamber walls (Walker et al. 2016a; Walker et al. 2016b).

Hall thrusters rely on externally applied electric and magnetic !elds for the creation of plasma and for expelling the ions of this plasma at high velocities to generate thrust. Electrons are emitted by an external source, generally a hollow cathode, to start the plasma discharge inside the thruster discharge channel via electron impact ionization of the neutral propellant gas. #e same electron source also provides electrons for the neutralization of the ion beam exiting the thruster. While the ions are axially accelerated by the applied electric !eld, the magnetic !eld causes the electrons to have a cycloid motion in the azimuthal direction due to their much lower mass. #e electrons expelled from the cathode track the magnetic !eld lines from the cathode to the thruster. As the magnetic !eld topology are formed with electromagnets orients electrons towards the inside of the channel, they experience cyclotron motion with a frequency, ωe = . Cyclotron motion frequency of the electrons is higher than the frequency of the ions. Besides, cyclotron frequency of electrons is higher than their collisional frequency, , such that ωe >> ve (Ahedo and Gallardo 2003). #e E × B dri% is generated in the discharge chamber and contributes to the Hall the region with the maximum magnetic &ux density (Xu and Walker 2014). #e Hall parameter, β, is de!ned by Eq. 1

$$\beta = \frac{\omega_e}{v_e} = \frac{eB}{m_e v_e} \qquad (1)$$

where me and e are the electron mass and electron charge, respectively. Since the electrons are well magnetized, in E × B dri%region, the Hall parameter has high values (Xu and Walker 2014). Figure 1 illustrates the paths of the electrons for a Hall thruster.

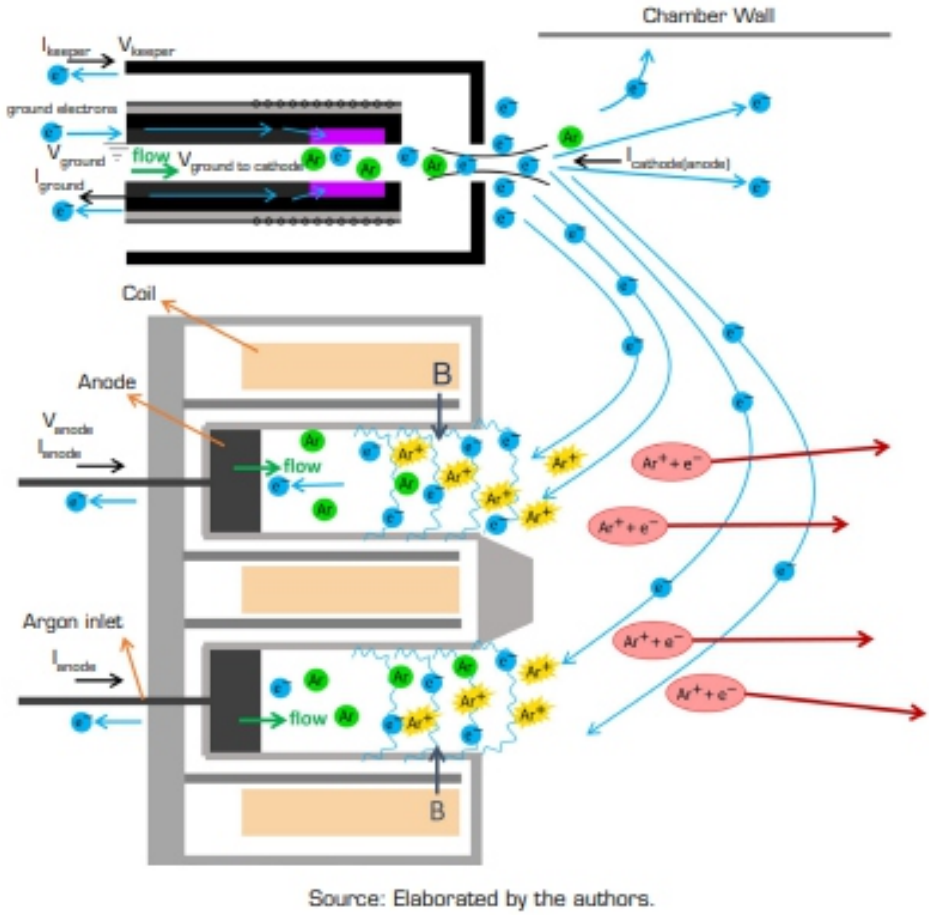

Figure 1. Schematic of the electron paths in a Hall thruster cathode system inside a vacuum chamber.

For Hall thrusters, the Hall parameter is large for the region where the magnetic &ux density is high while the electrical resistivity is also high in these regions with the limited electron &ow towards the anode in the channel. Furthermore, environments with di"erent surface potentials or grounding/&oating settings can alter the electron pathways resulting in a loss of the produced electrons. Since the magnetic !eld lines substantially a"ect the ionization and the extracted current from a discharge, the proper design of the magnetic !eld topology is crucial. #e challenges in the design of the electrical and magnetic circuit of the thruster largely stem from the anomalous behavior of the electrons within the channels (Mikellides and Ortega 2019). While this behavior presents a complexity for the design and modelling of Hall thrusters, simpli!ed assumptions can provide a way to estimate the thruster performance by macro-scale measurements that are readily made during tests, such as the measurements of voltages and currents. LaB6 cathode, also designed and developed at BUSTLab, was used as the cathode for the operation of this thruster (Kurt et al. 2017). #e details of the test setup and the equipment are discussed in the following section.

In this study, we aim to investigate the role of the chamber in estimating thruster e$ciency by providing a comparison between the grounded and the &oating electrical wiring con!gurations. #e HK40, an experimental SPT type Hall e"ect thruster which was built at the Bogazici University Space Technologies Laboratory (BUSTLab), was used as the test bed for the investigation. Alaboratory type LaB6 cathode, also designed and developed at BUSTLab, was used as the cathode for the operation of this thruster (Kurt et al. 2017). #e details of the test setup and the equipment are discussed in the following section.

EXPERIMENTAL SETUP

BUSTLab vacuum facility (Korkmaz 2015) is used for the experiments. #e vacuum chamber has a diameter of 1.5 m and a length of 2.7 m. Vacuum level on the order of 3 × 10−6 Torr is reached with the use of two 12 inch cryopumps without any gas &ow to the chamber. As the propellant, argon was supplied to the thruster (18 sccm) and to the cathode (2.2 sccm) through the chamber ports and controlled by a set of MKS &ow controllers. For this rate of propellant &ow to the thruster and cathode, the pressure of the chamber was measured to be 4.2 × 10−5 Torr during the tests. A Sorensen DCS600-1.7 was utilized for powering the cathode and a Glassman FL1250F1.2 power source was used for the thruster.

HK40 Hall Effect Thruster

HK40 is a prototype Hall thruster that utilizes a dielectric discharge chamber with outer diameter of 40 mm (Turan 2016). #e thruster employs !ve identical cylindrical electromagnets, each with a diameter of 1/2 inch and a length of 1 inch long electromagnets; one of these electromagnets are placed inside the coaxial channel and the remaining four are on the outside. A side view picture along with a rendering of the CAD drawing of the HK40 Hall thruster with the LaB6 hollow cathode are shown in Fig. 2.

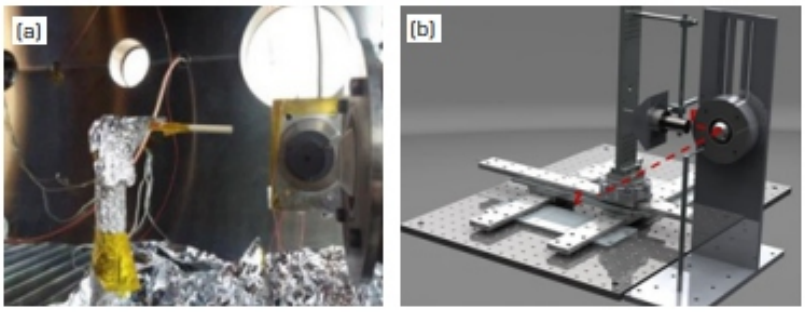

Source: Elaborated by the authors.

Figure 2. (a) HK40 Hall thruster and the LaB6 hollow cathode with the Langmuir probe (b) Illustration of the test assembly with the vacuum translational stage (dashed lines indicating the axial and radial directions)

BUSTLab Hollow Cathode

#e hollow cathode used for the operation of the HK40 Hall thruster utilizes a LaB6 tube with an inner diameter of 2 mm, outer diameter of 4 mm and length of 10 mm as the thermionic emission material. #e cathode tube of this hollow cathode is of graphite with an outer diameter of 6 mm and length of 48 mm. #is cathode has a unique heater assembly: tantalum wire of 0.25 mm diameter is wrapped around a shapal ceramic tube with external grooves of helical geometry. For electrical connection of the heater circuit, the tantalum wire is continued to wrap around the grooves on a graphite part that is placed coaxially over the cathode tube (Kurt et al. 2017; Kokal et al. 2021).

#e LaB6 insert placed in the cathode tube is the source of electrons leaving the cathode. #e insert is at ground potential as seen in Fig. 3. As the LaB6 insert starts emitting electrons, it will start attracting electrons from the ground since it is momentarily electron de!cient. As discussed in the next section, during the experiments, cathode current, which is generated by the electrons extracted from the ground, is measured.

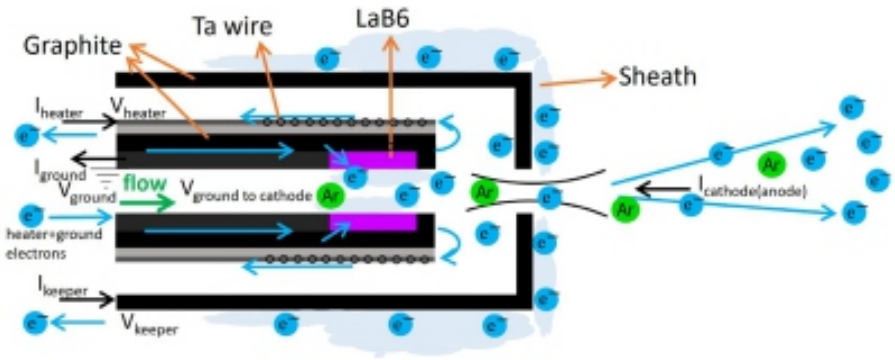

Source: Elaborated by the authors.

Figure 3. Schematic of electron extraction from LaB_6 cathode.

Langmuir Probe

A single Langmuir probe is used to measure the electron temperature and plasma potential of the thruster plume plasma. #is Langmuir probe employs a molybdenum rod with a diameter of 1 mm placed inside a single hole, 3.18 mm outer diameter alumina tube (Yildiz and Celik 2019). For biasing the probe electrode and measuring the current collected by the electrode, a Keithley 2410 sourcemeter is used.

Thrust Stand

#e thrust stand, built in-house at BUSTLab, utilizes an inverted pendulum mechanism (Kokal and Celik 2017; Kokal 2018) with two horizontal platforms and two pendulum arms. Counterweights are utilized to balance the weight of the thruster, as a result the e"ect of the thruster weight on thrust measurements is mitigated. #e pendulum mechanism is assembled with stainless steel &exures.

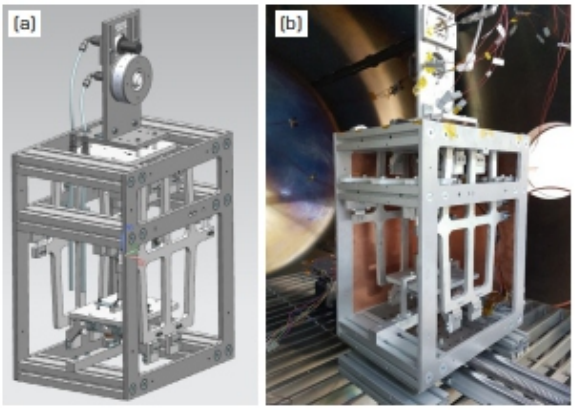

Source: Elaborated by the authors.

Figure 4. HK40 Hall thruster on the thrust stand.

COMPARISON OF TWO DIFFERENT WIRING CONFIGURATIONS

We introduce a circuit analogy that contains potentials and currents in the thruster-cathode-chamber system. #e resistances are de!ned between the potentials, which are represented in the voltage schematic as in Fig. 5. #e discharge potential (Vd) is the di"erence between the anode potential (Va) and the cathode potential (Vcg). #e plasma potential (Vp) is the voltage level that is experimentally determined in the plume region, where ion acceleration is !nalized. #e ions are accelerated with the beam potential (Vb), which is the voltage di"erence between the anode and plasma voltages. #e cathode coupling potential (Vc) is the di"erence of the plasma and the cathode potential.

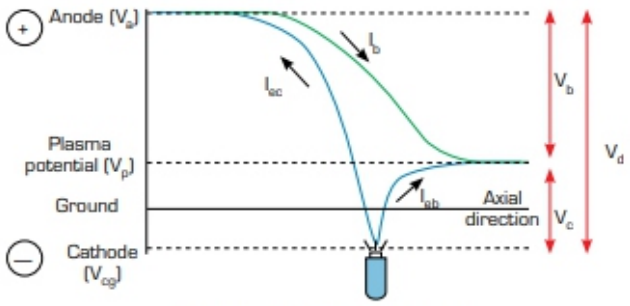

Source: Elaborated by the authors.

Figure 5. Hall thruster voltage schematic with corresponding currents.

Two representative schematics are introduced to illustrate the thruster-cathode-chamber system electrical circuits for laboratory and in-&ight conditions. In the grounded setup, the power supplies, which provide the anode and keeper voltages, are grounded to the vacuum chamber (Vg). A multimeter is placed between the cathode and the ground in order to measure the cathode to ground current g). In this setup, the cathode voltage (Vcg) is zero, therefore the anode voltage (Va) and the discharge voltage (Vd) are equal. #e value of the discharge voltage is read from the power supply. Figure 6 shows the de!ned potentials with resistances and currents for the grounded setup.

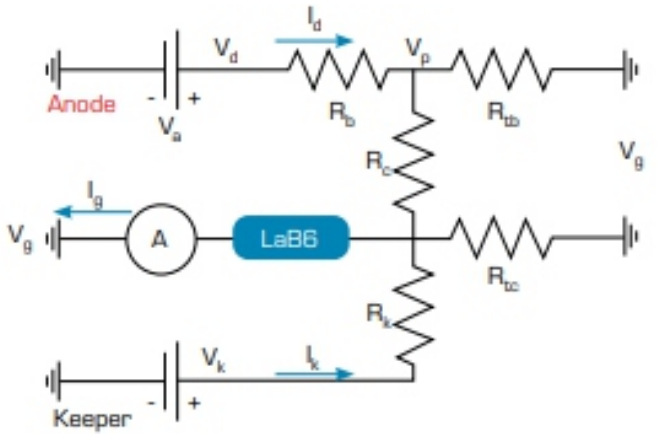

Figure 6. Schematic of the grounded setup electrical con!guration of thruster-cathode system.

#e anode and cathode form a closed circuit where Rb is the resistance between plasma and anode, Rc is the resistance between plasma and cathode (LaB6 insert) and Rk is the resistance between keeper and cathode (LaB6 insert). Here, the magnetic !eld topology in the discharge channel determines Rb and it is proportional to the square of the Hall parameter as in Eq. 1. Hence, the increased strength of the magnetic !eld increases Rb. #e cathode placement, as well as the topology of the external magnetic !eld, determines Rc. #e resistance inside the hollow cathode between the keeper electrode and the LaB6 insert material is represented by Rk. As the experiments are conducted in the vacuum chamber, the resistance between the thruster plume and vacuum chamber wall, Rtb, and the resistance between the cathode and the vacuum chamber wall, Rtc, are added to the system.

In the &oating con!guration, as depicted in Fig. 7, the negative leads of the anode and keeper power supplies, and the negative lead of the cathode heater circuit are all connected at a &oating common point ($oating ground). #e negative lead of the cathode heater circuit completes the circuit through the cathode insert material. A multimeter placed between the ground of the vacuum chamber and the &oating ground is used to measure the voltage Vcg between the &oating common ground voltage and the ground voltage (the ground of the vacuum chamber and hence the Earth). In the &oating con!guration, the cathode voltage Vcg is not zero, therefore the discharge voltage is equal to the di"erence between the anode voltage Va and the cathode voltage (Vcg). #is setup better resembles the electrical circuit of a thruster on a satellite, where the components of the system are powered with respect to Vcg instead of Earth's ground.

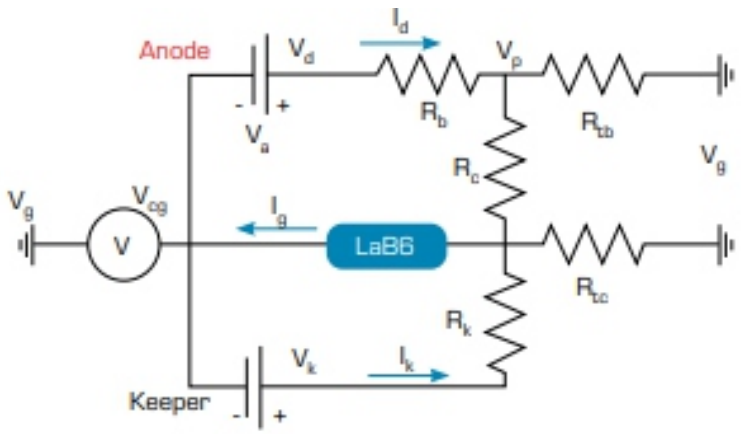

Source: Elaborated by the authors.

Figure 7. Schematic of the floating setup electrical configuration of the thruster-cathode system.

ESTIMATION OF THRUST AND EFFICIENCY

#e e$ciency and thrust of the thruster are estimated with the help of the introduced circuit analogy using readily measurable voltage and current values as well as the Langmuir probe measurements. In this section, thrust and e$ciency calculations are presented. For the grounded setup, the measured current between the LaB6 insert and the ground as depicted in Fig. 6 is used. Similarly, for the &oating setup, the measured voltage between the &oating common ground and the ground as depicted in Fig. 7 is used.

As stated earlier, tests are conducted with argon as the propellant with an anode propellant &ow rate of 18 sccm and cathode propellant &ow rate of 2.2 sccm. For the calculations, singly ionized argon ions are assumed. #e fraction of the propellant leaving the thruster as ions, namely the current e$ciency, ηi, was estimated to be in the range of 75-80% (Ross and King 2007). #e divergence half angle was taken to be 37 degrees (Turan 2016; Baird et al. 2021). #e beam divergence e$ciency, ηd, value was obtained from the cosine of this angle.

Calculating ef!ciency from the ground current#e ions are created inside the discharge channel and then accelerated towards the downstream plume region from the location where they are created. #e electric potential in the plume plasma is a"ected by the topology of the magnetic !eld, the electron current supplied from the cathode, the cathode position, and the characteristics of the discharge. Despite the electric potential of the region in the discharge channel where the ions are created slightly lower than the electric potential of the anode, the beam power can be estimated by Eq. 2:

$$P_b = I_b(V_a - V_p) = I_b(V_d - V_p) = I_b V_b \quad (2)$$

where the plasma potential, Vp, is measured with a Langmuir probe.

#e beam current (Ib), that is the current due to the expelled ions, is the di"erence between the discharge current (Id) and the portion of the cathode electron current backstreaming towards the anode (Iec) (Goebel and Katz 2008). #e discharge current is generated by the backstreaming electrons from the cathode and also by the ionization of the neutrals (Eq. 3):

$$I_d = I_{ec} + I_b \quad (3)$$

Where I ec, the backstreaming cathode electrons, is measured from the current drawn from the ground (see Fig. 6). One should also note that the same amount of electrons and ions are generated in the plasma discharge due to ionization (Eq. 4):

$$I_b = I_{ei} \quad (4)$$

where I ei is the electron current due to ionization. #e created ions are ejected towards the exit. Electrons move towards the anode as shown in Fig. 1. #rust in more general terms is de!ned by Eq. 5:

$$T = \dot{m}_i v_{avg} \quad (5)$$

where =nim. is the propellant mass &ow rate that is ionized, ni is the ionization e$ciency, and vavg is the mean value of velocity of ions in axial direction given by Eq. 6:

$$v_{avg} = \sqrt{n_d \frac{2_e(V_d - V_p)}{M_i}} \quad (6)$$

where Mi is the mass of an ion, ηd is the beam divergence coe$cient and e is the electron charge (Sommerville and King 2007). #e thrust is calculated by Eq. 7

$$T = \frac{I_b M_i}{e} \sqrt{n_d \frac{2_e(V_d - V_p)}{M_i}} \quad (7)$$

The efficiency is evaluated using Eq. 8:

$$n_{anode} = \frac{n_i n_d \dot{m}_i e(V_d - V_p)}{M_i P_{anode}} \quad (8)$$

where ·mi is the ion mass &ow rate and Panode = Id Vd is the total anode power.

Calculating ef!ciency from cathode to ground voltage

For the foating setup, as seen in Fig. 7, the cathode to ground voltage, Vcg, which is the cathode voltage, is measured. For this con!guration, the discharge current (Id) will again be the total of the beam current (Ib) and the current due to the backstreaming electrons, Iec.

As discussed earlier, a majority of the electrons leave the cathode exit into the far-!eld plume for the neutralization of the beam ions. #e remainder of the electrons backstream towards the anode causing the ionization of the neutral propellant released from the anode region. In order to fully resolve this electron current transport, a fast, spatial sweeping probe is needed, yet it is experimentally challenging. #us, based on the studies in the literature (McDonald and Gallimore 2011; Smith and Cappelli 2010), the percentage of the backstreaming electrons was taken to be on the order of 20% of the discharge current.#e electric potential that causes the acceleration of the ions is the di"erence between the plasma voltage and applied anode voltage as shown in Fig. 5. Since the discharge voltage is with respect to the &oating ground, the cathode to ground voltage is also needed to be added to the discharge voltage to obtain the anode voltage (Eq. 9).

$$V_b = V_d + V_{cg} - V_p \tag{9}$$

The thrust is calculated by Eq. 10:

$$T = \frac{I_b M_i}{e}\sqrt{n_d \frac{2e(V_d+V_{cg}-V_p)}{M_i}}$$

Hence the thrust efficiency is:

$$n_{anode} = \frac{n_i n_d \dot{m}_i e(V_d+V_{cg}-V_p)}{M_i P_{anode}}$$

where I_d V_d is the total anode power, P_{anode}.

RESULTS AND DISCUSSIONS

As described earlier, the thruster magnetic !eld is created by four outer coils and one inner coil. For Hall thrusters, a high Hall parameter, β, with a high magnetic !eld B results in an increase in the beam resistance (Rb) in the acceleration region. #erefore, the potential di"erence between the cathode and the anode is concentrated in the acceleration region. In the experiments, for both con!gurations, the thruster is operated at discharge voltage of 200V and discharge current of 1.2A. For these conditions, the calculated e$ciency and thrust values are presented in Table 1.

Table 1. Detailed comparison of calculated values of HK40 Hall thruster for grounded and &oating wiring con!gurations.

Parameter	Grounded	Floating
Plasma Potential, V_p	25 V	26 V
Cathode Voltage, V_{cg}	0 V	-27 V
Backstreaming Current, I_{ec}	0.4 A	0.24 A*
Thrust, T	8.2 mN	9.0 mN
Efficiency, η_{anode}	0.21	0.26

*The backstreaming electron current fraction is taken to be 20% of the total discharge current (McDonald and Gallimore 2011).

Source: Elaborated by the authors.

For the grounded setup, the e$ciency and thrust values were calculated using Eqs. 7 and 8. For this setup, as described earlier, the power supplies were grounded, and the current drawn from the ground was measured using a multimeter serially connected between the return wire of the heater circuit and the ground. #e plasma potential in the plume region wa measured using a single Langmuir probe.For the &oating setup tests, the thrust was calculated using Eq. 10 by measuring the cathode to ground voltage and the e$ciency was calculated using Eq. 11. During the &oating setup experiments, all the power supplies were connected to a common ground as depicted in Fig. 7. When the calculated values are compared, it is observed that the &oating setup yielded higher predicted thrust and e$ciency values compared to the grounded setup as seen in Table 1.For the &oating setup, thrust measurements were conducted with the in-house built thrust stand. As seen in Table 2, the calculated and measured values showed di"erences for both thrust and e$ciency. Although the &oating setup better represents satellite operation in space, vacuum chamber walls a"ect the electron pathways during the tests. In the &oating setup, the cathode has a negative voltage, thus the chamber walls attract a portion of the electrons. However, in the grounded setup, cathode voltage is kept at ground voltage of the vacuum tank walls, therefore electron current from the cathode to the chamber walls is expected to be smaller, which may present a better representation of space conditions, as in space conditions electron pathways through Rtb and Rtcresistances do not exist (see Fig. 7). #is is also a loss mechanism as the electrons generated inside the cathode are wasted without being e$ciently utilized for ionization or neutralization purposes. #is is one plausible explanation for why the measured thrust is lower than the calculated value. One also must note that there is a ± 0.3mN uncertainty in thrust measurements. In addition, some of the assumptions such as the beam divergence angle can result in an over-estimation for the calculated thrust values.

Table 2. Comparison of calculated and measured values of HK40 Hall thruster for &oating wiring con!guration.

Parameter	Calculated	Measured
Thrust, T	9.0 mN	8.7 ± 0.3 mN
Efficiency, η_{anode}	0.26	0.24 ± 0.01

Source: Elaborated by the authors.

Due to the decrease in the magnetic !eld intensity away from the thruster, the current pathways for the electrons may change towards the thruster body for the region near to the discharge channel exit or towards the vacuum chamber walls for the regions away from the thruster. As a result of such electron recombination pathways, di"erent e$ciency and thrust values can be obtained for the ground and in space operations as observed in this study.

CONCLUSIONS

#is study presents the investigation of the e"ects of wiring con!guration of the thruster-cathode-chamber system using two di"erent grounding con!gurations on the operational characteristics of a prototype Hall thruster, HK40. Without considering the inherently complex electron pathways, we provided a macro-scale resistance analogy regarding the changes in the electrical potentials and measured currents to interpret thruster performance. #e thrust and e$ciency of the thruster were estimated with the help of the introduced circuit analogy using readily measurable voltage and current values as well as the Langmuir probe measurements. #e theoretical predictions were also compared with the thrust stand measurements for the &oating con!guration since it presents a comparison with space operation. We estimated the thrust and e$ciency with 3.4% and 8.3% uncertainty, respectively while operating the thruster at 200V of discharge voltage and 1.2A of discharge current. Our representative method can help understand the electron pathways through resistances, since we already measure voltages and currents during tests.

Future work would be operating the thruster in a wider range to validate its operation and reducing the number of assumptions in our calculations a%er integrating plume angle measurements with a Faraday probe.

CONFLICT OF INTEREST

Nothing to declare.

AUTHOR CONTRIBUTIONS

Conceptualization: Turan N and Kokal U; Data curation: Turan N and Kokal U; Formal analysis: Turan

N and Kokal U; Acquisition of funding: Celik M; Research: Turan N, Kokal U and Celik M; Methodology: Turan N, Kokal U and Celik M; Project administration: Celik M; Supervision: Celik M; Validation: Turan N and Kokal U; Visualization: Turan N and Kokal U; Writing - Preparation of original dra!: Celik M, Kokal U and Turan N; Writing - Proofreading and editing: Celik M, Kokal U and Turan N.

FUNDING

Scienti!c and Technological Research Council of Turkey, https://doi.org/10.13039/501100004410. Grant No: 214M572

ACKNOWLEDGMENTS

The authors would like to thank Professor Huseyin Kurt of Istanbul Medeniyet University for his contributions to the experimental setup and tests.

REFERENCES

1. Ahedo E, Gallardo JM (2003) Scaling down Hall #rusters. Paper presented at 28th Electric Propulsion Conference. IEPC; Toulouse, France.

2. Baird M, Kerber T, McGee-Sinclair R, Lemmer K (2021) Plume Divergence and Discharge Oscillations of an Accessible Low Power Hall E"ect #ruster. Appl Sci 11(4):1973. https://doi.org/10.3390/app11041973

3. Brophy JR, Friedman L, Culick F (2012) Asteroid Retrieval Feasibility. Paper presented at 2012 IEEE Aerospace Conference. IEEE; Big Sky, United States. https://doi.org/10.1109/AERO.2012.6187031

4. Brown DL, Gallimore AD (2011) Evaluation of Facility E"ects on Ion Migration in a Hall #ruster Plume. J Propuls Power 27(3):573-585. https://doi.org/10.2514/1.B34068

5. Cichocki F, Merino M, Ahedo E (2020) #ree-Dimensional Geomagnetic Field E"ects on a Plasma #ruster Plume Expansion. Acta Astronautica 175:190-203. https://doi.org/10.1016/j.actaastro.2020.05.019

6. Diamant KD, Liang R, Corey RL (2014) #e E"ect of Background Pressure on SPT-100 Hall #ruster Performance. Paper presented at 50th AIAA/ASME/SAE/ASEE Joint Propulsion Conference. AIAA; Cleveland, United States. https://doi.org/10.2514/6.2014-3710

7. Frieman JD, King ST, Walker MLR, Khayms V, King D (2014) Role of a Conducting Vacuum Chamber in the Hall E"ect #ruster Electrical Circuit. J Propuls Power 30(6):1471-1479. https://doi.org/10.2514/1.B35308

8. Frieman JD, Walker JA, Walker MLR, Khayms V, King DQ (2016) Electrical Facility E"ects on Hall #ruster Cathode Coupling: Performance and Plume Properties. J Propuls Power 32(1):251-264.

https://doi.org/10.2514/1.B35683

9. Goebel DM, Katz I (2008) Fundamentals of Electric Propulsion: Ion and Hall #rusters. Hoboken: John Wiley & Sons. https://doi.org/10.1002/9780470436448

10. Huang W, Kamhawi H, Lobbia RB, Brown DL (2014) E"ect of Background Pressure on the Plasma Oscillation Characteristics of the HiVHAc Hall #ruster. Paper presented at 50th AIAA/ASME/SAE/ASEE Joint Propulsion Conference. AIAA; Cleveland, United States. https://doi.org/10.2514/6.2014-3708

11. Huo Y (2022) Space Broadband Access: #e Race Has Just Begun. Computer 55(7):38-45. https://doi.org/10.1109/MC.2022.3160472

12. Kokal U (2018) Development of a Mili-Newton Level #rust Stand for #rust Measurements of Electric Propulsion Systems and UK90 Hall E"ect #ruster (MS thesis). Istanbul: Bogazici University.

13. Kokal U, Celik M (2017) Development of a Mili-Newton Level #rust Stand for #rust Measurements of Electric Propulsion Systems. Paper presented at 2017 8th International Conference on Recent Advances in Space Technologies (RAST). IEEE; Istanbul, Turkey. https://doi.org/10.1109/RAST.2017.8002970

14. Kokal U, Turan N, Celik M (2021) #ermal Analysis and Testing of Di"erent Designs of LaB6 Hollow Cathodes to be Used in Electric Propulsion Applications. Aerospace 8(8):215. https://doi.org/10.3390/aerospace8080215

15. Korkmaz O, Jahanbakhsh S, Celik M, Kurt H (2015) Space Propulsion Research Vacuum Facility of the Bogazici University Space Technologies Laboratory. Paper presented at 2015 7th International Conference on Recent Advances in Space Technologies (RAST). IEEE; Istanbul, Turkiye. https://doi.org/10.1109/RAST.2015.7208420

16. Kurt H, Kokal U, Turan N, Celik M (2017) Note: Coaxial-Heater Hollow Cathode. Rev Sci Instrum 88(6):066103. https://doi.org/10.1063/1.4986111

17. Lev D, Myers RM, Lemmer KM, Kolbeck J, Koizumi H, Polzin K (2019) #e Technological and Commercial Expansion of Electric Propulsion. Acta Astronautica 159:213-227. https://doi.org/10.1016/j.actaastro.2019.03.058

18. Levchenko I, Xu S, Teel G, Mariotti D, Walker MLR, Keidar M (2018) Recent Progress and Perspectives of Space Electric Propulsion Systems Based on Smart Nanomaterials. Nat Commun 9(1):879. https://doi.org/10.1038/s41467-017-02269-7

19. MacDonald-Tenenbaum N, Pratt Q, Nakles M, Pilgram N, Holmes M, Hargus Junior W (2019) Background Pressure E"ects on Ion Velocity Distributions in an SPT-100 Hall #ruster. J Propuls Power 35(2):403-412. https://doi.org/10.2514/1.B37133

20. Martinez-Sanchez M, Pollard JE (1998) Spacecra% Electric Propulsion-An Overview. J Propuls Power 14(5):688-699. https:// doi.org/10.2514/2.5331

21. Mazou"re S (2016) Electric Propulsion for Satellites and Spacecra%: Established Technologies and Novel Approaches. Plasma Sources Sci Technol 25(3):033002. https://doi.org/10.1088/0963-0252/25/3/033002

22. McDonald MS, Gallimore AD (2011) Electron Trajectory Simulation in Experimental Hall #ruster Fields. Paper presented at 32nd International Electric Propulsion Conference. IEPC; Wiesbaden, Germany. [accessed 2023 Jan. 12]. https://pepl.engin.umich.edu/pdf/IEPC-2011-243.pdf

23. Mikellides IG, Ortega AL (2019) Challenges in the Development and Veri!cation of First-Principles Models in Hall-E"ect #ruster Simulations that are Based on Anomalous Resistivity and Generalized Ohm's Law. Plasma Sources Sci Technol 28(1): 014003. https://doi.org/10.1088/1361-6595/aae63b

24. Nakles MR, Hargus Junior WA (2011) Background Pressure E"ects on Ion Velocity Distribution within a Medium-Power Hall #ruster. J Propuls Power 27(4):737-743. https://doi.org/10.2514/1.48027

25. Ortega AL, Mikellides IG, Chaplin VH, Snyder JS, Lenguito G (2020) Facility Pressure E"ects on a Hall #ruster with an External Cathode: I. Numerical Simulations Plasma Sources Sci Technol 29(3):035011. https://doi.org/10.1088/1361-6595/ab6c7e

26. Potrivitu G-C, Sun Y, Rohaizat MWA, Cherkun O, Xu L, Huang S, Xu S (2020) A Review of Low-Power Electric Propulsion Research at the Space Propulsion Centre Singapore. Aerospace 7(6):67. https://doi.org/10.3390/aerospace7060067

27. Ross JL, King LB (2007) Energy E$ciency in Low Voltage Hall #rusters. Paper presented at 43rd AIAA/ASME/SAE/ASEE Joint Propulsion Conference & Exhibit. AIAA; Cincinnati, United States. https://doi.org/10.2514/6.2007-5179

28. Smith AW, Cappelli MA (2010) Single Particle Simulations of Electron Transport in the Near-Field of Hall #rusters. J Phys D: Appl Phys 43(4):045203. https://doi.org/10.1088/0022-3727/43/4/045203 Sommerville JD, King LB (2007) E"ect of Cathode Position on Hall-E"ect #ruster Performance and Cathode Coupling Voltage. Paper presented at 43rd AIAA/ASME/SAE/ASEE Joint Propulsion Conference & Exhibit, AIAA; Cincinnati, United States. https://doi.org/10.2514/6.2007-5174

29. Turan N (2016) Experimental Investigation of the E"ects of Cathode Position on HK40 Hall E"ect #ruster Performance and Cathode Coupling (PhD thesis). Istanbul: Bogazici University

30. Walker JA, Frieman JD, Walker MLR, Khayms V, King D, Peterson PY (2016a) Electrical Facility E"ects on Hall-E"ect-#ruster Cathode Coupling: Discharge Oscillations and Facility Coupling. J Propuls Power 32(4):844-855. https://doi.org/10.2514/1.B35835

31. Walker JA, Langendorf SJ, Walker MLR, Khayms V, King D, Pertson P (2016b) Electrical Facility E"ects on Hall Current #rusters: Electron Termination Pathway Manipulation. J Propuls Power 32(6):1365-1377. https://doi.org/10.2514/1.B35904

32. Walker MLR (2005) E"ects of Facility Backpressure on the Performance and Plume of a Hall

#ruster (master's thesis). Ann Arbor: University of Michigan.

33. Xu KG, Walker MLR (2014) E"ect of External Cathode Azimuthal Position on Hall-E"ect #ruster Plume and Diagnostics. J Propuls Power 30(2):506-513. https://doi.org/10.2514/1.B34980

34. Yildiz MS, Celik M (2019) Plume Diagnostics of BUSTLab Microwave Electrothermal #ruster using Langmuir and Faraday Probes. Plasma Sci Technol 21(4):045505. https://doi.org/10.108

Instructions for Authors

Essentials for Publishing in this Journal

1 Submitted articles should not have been previously published or be currently under consideration for publication elsewhere.

2 Conference papers may only be submitted if the paper has been completely re-written (taken to mean more than 50%) and the author has cleared any necessary permission with the copyright owner if it has been previously copyrighted.

3 All our articles are refereed through a double-blind process.

4 All authors must declare they have read and agreed to the content of the submitted article and must sign a declaration correspond to the originality of the article.

Submission Process

All articles for this journal must be submitted using our online submissions system. http://enrichedpub.com/ . Please use the Submit Your Article link in the Author Service area.

Manuscript Guidelines

The instructions to authors about the article preparation for publication in the Manuscripts are submitted online, through the e-Ur (Electronic editing) system, developed by **Enriched Publications Pvt. Ltd**. The article should contain the abstract with keywords, introduction, body, conclusion, references and the summary in English language (without heading and subheading enumeration). The article length should not exceed 16 pages of A4 paper format.

Title

The title should be informative. It is in both Journal's and author's best interest to use terms suitable. For indexing and word search. If there are no such terms in the title, the author is strongly advised to add a subtitle. The title should be given in English as well. The titles precede the abstract and the summary in an appropriate language.

Letterhead Title

The letterhead title is given at a top of each page for easier identification of article copies in an Electronic form in particular. It contains the author's surname and first name initial .article title, journal title and collation (year, volume, and issue, first and last page). The journal and article titles can be given in a shortened form.

Author's Name

Full name(s) of author(s) should be used. It is advisable to give the middle initial. Names are given in their original form.

Contact Details

The postal address or the e-mail address of the author (usually of the first one if there are more Authors) is given in the footnote at the bottom of the first page.

Type of Articles

Classification of articles is a duty of the editorial staff and is of special importance. Referees and the members of the editorial staff, or section editors, can propose a category, but the editor-in-chief has the sole responsibility for their classification. Journal articles are classified as follows:

Scientific articles:

1. Original scientific paper (giving the previously unpublished results of the author's own research based on management methods).

2. Survey paper (giving an original, detailed and critical view of a research problem or an area to which the author has made a contribution visible through his self-citation);

3. Short or preliminary communication (original management paper of full format but of a smaller extent or of a preliminary character);

4. Scientific critique or forum (discussion on a particular scientific topic, based exclusively on management argumentation) and commentaries. Exceptionally, in particular areas, a scientific paper in the Journal can be in a form of a monograph or a critical edition of scientific data (historical, archival, lexicographic, bibliographic, data survey, etc.) which were unknown or hardly accessible for scientific research.

Professional articles:

1. Professional paper (contribution offering experience useful for improvement of professional practice but not necessarily based on scientific methods);
2. Informative contribution (editorial, commentary, etc.);
3. Review (of a book, software, case study, scientific event, etc.)

Language

The article should be in English. The grammar and style of the article should be of good quality. The systematized text should be without abbreviations (except standard ones). All measurements must be in SI units. The sequence of formulae is denoted in Arabic numerals in parentheses on the right-hand side.

Abstract and Summary

An abstract is a concise informative presentation of the article content for fast and accurate Evaluation of its relevance. It is both in the Editorial Office's and the author's best interest for an abstract to contain terms often used for indexing and article search. The abstract describes the purpose of the study and the methods, outlines the findings and state the conclusions. A 100- to 250-Word abstract should be placed between the title and the keywords with the body text to follow. Besides an abstract are advised to have a summary in English, at the end of the article, after the Reference list. The summary should be structured and long up to 1/10 of the article length (it is more extensive than the abstract).

Keywords

Keywords are terms or phrases showing adequately the article content for indexing and search purposes. They should be allocated heaving in mind widely accepted international sources (index, dictionary or thesaurus), such as the Web of Science keyword list for science in general. The higher their usage frequency is the better. Up to 10 keywords immediately follow the abstract and the summary, in respective languages.

Acknowledgements

The name and the number of the project or programmed within which the article was realized is given in a separate note at the bottom of the first page together with the name of the institution which financially supported the project or programmed.

Tables and Illustrations

All the captions should be in the original language as well as in English, together with the texts in illustrations if possible. Tables are typed in the same style as the text and are denoted by numerals at the top. Photographs and drawings, placed appropriately in the text, should be clear, precise and suitable for reproduction. Drawings should be created in Word or Corel.

Citation in the Text

Citation in the text must be uniform. When citing references in the text, use the reference number set in square brackets from the Reference list at the end of the article.

Footnotes

Footnotes are given at the bottom of the page with the text they refer to. They can contain less relevant details, additional explanations or used sources (e.g. scientific material, manuals). They cannot replace the cited literature.
The article should be accompanied with a cover letter with the information about the author(s): surname, middle initial, first name, and citizen personal number, rank, title, e-mail address, and affiliation address, home address including municipality, phone number in the office and at home (or a mobile phone number). The cover letter should state the type of the article and tell which illustrations are original and which are not.

Address of the Editorial Office:

Enriched Publications Pvt. Ltd.
S-9,IInd FLOOR, MLU POCKET,
MANISH ABHINAV PLAZA-II, ABOVE FEDERAL BANK,
PLOT NO-5, SECTOR -5, DWARKA, NEW DELHI, INDIA-110075,
PHONE: - + (91)-(11)-45525005